



HAL
open science

A stable, unified model for resonant Faraday cages

Bérangère Delourme, Eric Lunéville, Jean-Jacques Marigo, Agnès Maurel,
Jean-François Mercier, Kim Pham

► **To cite this version:**

Bérangère Delourme, Eric Lunéville, Jean-Jacques Marigo, Agnès Maurel, Jean-François Mercier, et al.. A stable, unified model for resonant Faraday cages. Proceedings of the Royal Society A: Mathematical, Physical and Engineering Sciences, 2021, 477 (2245), pp.20200668. 10.1098/rspa.2020.0668 . hal-03370501

HAL Id: hal-03370501

<https://hal.science/hal-03370501v1>

Submitted on 20 Oct 2021

HAL is a multi-disciplinary open access archive for the deposit and dissemination of scientific research documents, whether they are published or not. The documents may come from teaching and research institutions in France or abroad, or from public or private research centers.

L'archive ouverte pluridisciplinaire **HAL**, est destinée au dépôt et à la diffusion de documents scientifiques de niveau recherche, publiés ou non, émanant des établissements d'enseignement et de recherche français ou étrangers, des laboratoires publics ou privés.

A stable, unified, model for resonant Faraday cages

October 20, 2021

B. Delourme¹, E. Lunéville², J.-J. Marigo³, A. Maurel⁴,
J.-F. Mercier² and K. Pham⁵ ¹LAGA, Université Paris 13, Villetaneuse,
France,

²Poems, CNRS, ENSTA ParisTech, INRIA, 828 Bd des Maréchaux, 91762
Palaiseau, France,

³LMS, CNRS, Ecole Polytechnique, 91120 Palaiseau, France,

⁴Institut Langevin, CNRS, ESPCI ParisTech, 1 rue Jussieu, 75005 Paris,
France,

⁵IMSIA, CNRS, ENSTA ParisTech, 828 Bd des Maréchaux, 91732 Palaiseau,
France, mathematical physics, waves

asymptotic analysis, high order homogenization, homogenized bound-
ary conditions, thin periodic interface B. Delourme delourme@math.univ-
paris13.fr

Abstract

We study effective transmission conditions able to reproduce the effect of a periodic array of Dirichlet wires on wave propagation in particular when the array delimits an acoustic Faraday cage able to resonate. In the study of Hewett and Hewitt. 2016 *Proc. R. Soc. A*, **472: 20160062**, different transmission conditions emerge from the asymptotic analysis whose validity depends on the frequency, specifically to the distance to a resonance frequency of the cage. In practice, dealing with such conditions is tricky especially if the problem is set in the time-domain. In the present study, we demonstrate the validity of a simpler *unified* model derived in Marigo and Maurel 2016. *Proc. R. Soc. A*, **472: 20160068**, *unified* meaning valid whatever the distance to the resonance frequencies. The effectiveness of the model is discussed in the harmonic regime thanks to explicit solutions. It is also exemplified in the time domain where a formulation guarantying stability of the numerical scheme has been implemented.

1 Introduction

A Faraday's cage is a cavity whose metallic boundary acts as a shield against external electrical discharges. When this boundary is punctured the shielding is not perfect anymore. Originally set in the static case, Faraday cage structures have been studied in electromagnetism for applications to filtering and shielding by gratings and grids. In this context, the question of the radiation leakage for instance from microwave oven doors has been addressed theoretically [1, 2, 3] and experimentally [4]. More recently, the problem has been revisited and extended to the acoustic case *i.e.* governed by Helmholtz equation [5, 6, 7] and to the electromagnetic case, *i.e.* governed by Maxwell's equations [8]. The aim is to evaluate the effectiveness of the shielding when waves propagate outside a cage made of a periodic arrangement of wires; in two-dimensions, the distance between the wires is h and their typical extend is e . The low frequency regime is considered *i.e.* $kh = O(\varepsilon)$ and $\varepsilon \ll 1$, where k is the typical wavenumber imposed by the source. Besides, in most of these studies, *thin wire* approximation is used which means that $\frac{e}{h} \ll 1$ hence the shielding is controlled by the number N of wires per unit length. Martin derived explicit solutions using multiple scattering theory for N point like wires evenly distributed on a line (not a cage) or on a large circle (a cage) [5]. For a cage, Hewett and co-authors showed that the asymptotic limit of large N results in a continuum model involving homogeneized transmission conditions across an effective interface [6, 7]. For *thin wires*, these conditions are derived using the specific scaling $(\frac{e}{h}) = O(e^{-\frac{c}{\varepsilon}})$ for every $c > 0$, introduced in [9] for thin Dirichlet fibres in a large volume. This scaling allows the coupling between the two sides of the array to be captured in the *limit problem* that is the zero order problem provided by the asymptotic analysis. This is a key point in the present context. Indeed, for *thick wires* with $(\frac{e}{h}) = O(1)$, the coupling cannot be captured by the limit problem; at the zero order, the array is crudely replaced by a Dirichlet wall. (In [8] this is used to discriminate between different geometries of arrays those producing an efficient shielding.) The coupling is captured at the first order. For the problem of scattering by a linear array in free space considered in [5], this is incidental: the zero order model predicts zero transmission and the first order model a small transmission. However, when the array delimits a cavity, the limit problem is ill-posed at the resonances of the close cavity. To overcome this difficulty Hewett and Hewitt derived a model made of two different conditions, ones being valid far from the resonances and the others near the resonances [7]. The problem has been approached differently by Marigo and Maurel [10, 11] who derived effective conditions without considering a spe-

cific wave problem. These *unified* conditions, which gather the zero and first order conditions, have been further applied to the scattering by a linear array in the free space (not a cage) [10] and to the scattering by the same array at a distance D of a Dirichlet wall with $kD = O(1)$ (a one-dimensional cage), see Appendix B in [11]. The underlying idea is that the effective conditions remain valid in any wave problem as long as this problem does not involve a length comparable to that of the array spacing (the microstructure). We can notice that the same idea applies to classical transmission conditions across a flat interface : while no interface is truly flat in the least at the atomic scale, it is commonly admitted that what matters is that it appears to be flat at the scale of the wavelength. Accordingly their validity is not interrogated whenever a new problem is considered. Intuitively this should be true after any homogenization process if the resulting conditions have the same, good, properties as the actual ones. In [11] the construction of *unified* conditions, avoiding an iterative resolution, provides a well-posed effective problem. This being said, well-posedness does not implies effectiveness of the model to approximate the actual solution. We address this question in the case of a cage by constructing asymptotic expansions of the solutions of the actual problem and of the unified, approximate, problem. By construction the expansions coincide far from the resonances; more interestingly they also coincide near and at the resonances. It is a good news for homogenization that no complication occurs in a simple configuration where the unique additional length scale, that of the resonant cavity, is at the largest, wavelength, scale. More generally, this interrogates the pertinence of an iterative resolution which reconstitutes faithfully the expansion of the solution. Indeed, such an expansion can fail in satisfying basic conservation laws. In contrast, a model using unified conditions is shown to enjoy the same good properties of the actual problem (conservation of the fluxes in the harmonic regime and conservation of the energy in the time domain).

The rest of the paper is organized as follows. In §2, we remind the results of the homogenization procedure for an array in the free space. The result is the zero and first order transmission conditions as used in an iterative resolution and the construction of unified, up-to-first order, conditions. We move on to the Faraday cage in §3 where we prove that the solution of the unified problem efficiently approximates the actual solution far, near and on the resonances. Numerical results are collected in §4 and 5. In the harmonic regime, §4, explicit solutions of the effective models are available. We illustrate the effectiveness of our (unified) model that we compare with the 3 solutions resulting from an iterative resolution being piecewise-valid far, near and on resonance. (It is shown that the 3 solutions coincide with

Taylor expansions of the unified one.) To anticipate, the advantage of the unified solution can be summarized by comparing the forthcoming figures 5 and 7. In §5 we consider the transient regime which poses the problem of the stability of effective models. The initial formulation of the unified model is shown to belong to a family of formulations with the same asymptotic limit. We show that only a part of this family ensures stability of the model when it is associated with a law of energy conservation involving a positive effective energy. The numerical implementation of a stable effective model allows us to show its effectiveness by comparison with direct numerics. We also illustrate the problem of numerical instability for unstable formulation and the link with the behavior of the effective, interfacial, energy. Concluding remarks and extensions of the present work are given in §6. We also collect additional calculations and results in 4 appendices.

We denote (p, \mathbf{u}) the fields satisfying the wave equation in the time domain

$$\frac{\partial \mathbf{u}}{\partial t} = -\nabla p, \quad \frac{\partial p}{\partial t} + \operatorname{div} \mathbf{u} = 0, \quad (1)$$

(the wave speed is $c = 1$), and in the harmonic regime with time dependence $e^{-i\omega t}$, p satisfies the Helmholtz equation

$$\Delta p + k^2 p = 0, \quad (2)$$

with $k = \frac{\omega}{c}$. We denote $\mathbf{x} = (x_1, x_2)$ the spatial coordinate and we consider an array of wires whose boundaries are associated with Dirichlet boundary condition $p = 0$. The array with spacing h is comprised in $x_1 \in (-e_1, e_1)$ and it can be unbounded or bounded along x_2 . Within the array, a wire has typical extends $2e_1 = O(h)$ along x_1 and $2e_2 = O(h)$ along x_2 (figure 1). To conduct the asymptotic analysis, we introduce the non-dimensional coordinate $\mathbf{x} = \frac{\mathbf{x}}{L}$, $\mathbf{x} = (x_1, x_2)$, with L of the order of a typical wavelength imposed by the source, and we introduce the small parameter

$$\varepsilon = \frac{h}{L} \ll 1.$$

2 Reminder: a linear array in the free space (not a cage)

Here we consider the free space and an array of wires evenly distributed on the interface $\Gamma = \{(0, x_2) \in \mathbb{R}^2, x_2 \in \mathbb{R}\}$, hence unbounded along x_2 .

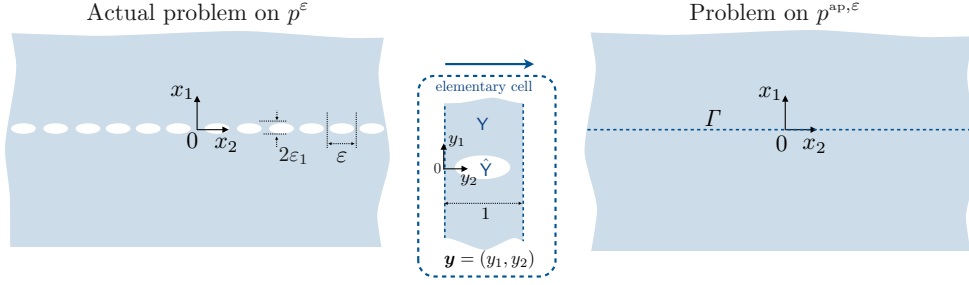


Figure 1: A linear array in free space (not a cage) – Left panel : the actual problem on p^ε in rescaled coordinate $\mathbf{x} = \frac{\mathbf{x}}{L}$. Right panel : the resulting effective problem on p^{ap} . The asymptotic homogenization, symbolized with the arrow involves elementary problems on (Q^-, Q^+) set in an elementary cell Y containing a single wire.

2.1 Iterative or unified transmission conditions

The asymptotic analyses conducted in [7] and in [10, 11] are basically identical and they provide the same results. With $p = p_0 + \varepsilon p_1 + O(\varepsilon^2)$, the zero-order term p_0 is found to satisfy the wave equation (1) in the transient regime or (2) in the harmonic regime with boundary conditions

$$p_0(0^\pm, x_2) = 0. \quad (3)$$

The first-order term p_1 is found to satisfy (1) or (2) with boundary conditions fed by p_0 , specifically

$$\begin{cases} p_1(0^-, x_2) = \mathcal{A} \frac{\partial p_0}{\partial x_1}(0^+, x_2) - \mathcal{B} \frac{\partial p_0}{\partial x_1}(0^-, x_2), \\ p_1(0^+, x_2) = \mathcal{B} \frac{\partial p_0}{\partial x_1}(0^+, x_2) - \mathcal{A} \frac{\partial p_0}{\partial x_1}(0^-, x_2). \end{cases} \quad (4)$$

The two real constants $(\mathcal{A}, \mathcal{B})$ are given by the elementary solution Q^+ set in rescaled coordinate $\mathbf{y} = \frac{\mathbf{x}}{\varepsilon}$ in the domain $Y = \left\{ (y_1, y_2) \in \mathbb{R} \times (0, 1) \setminus \widehat{Y} \right\}$, where $\widehat{Y} \subset \left(-\frac{\varepsilon_1}{h}, \frac{\varepsilon_1}{h}\right) \times (0, 1)$ is a canonical wire that we suppose symmetric with respect to the axis of equation $y_1 = 0$ (inset of figure 1). The elementary solution Q^+ is the 1-periodic *w.r.t* to y_2 solution to

$$\Delta Q^+ = 0, \quad \text{in } Y, \quad Q^+ = 0 \quad \text{on } \partial \widehat{Y}, \quad \text{and} \quad \lim_{y_1 \rightarrow -\infty} \nabla Q^+ = \mathbf{0}, \quad \lim_{y_1 \rightarrow +\infty} \nabla Q^+ = \mathbf{e}_1, \quad (5)$$

and the constants \mathcal{B} and \mathcal{A} are defined by

$$Q^+ \underset{y_1 \rightarrow -\infty}{\sim} \mathcal{A}, \quad Q^+ \underset{y_1 \rightarrow +\infty}{\sim} y_1 + \mathcal{B}. \quad (6)$$

A usual resolution consists in solving the problem on p_0 with (3), then that on p_1 using (4); we call the conditions (3) and (4) *iterative transmission conditions*. Following [12, 13, 14], *unified transmission conditions* are constructed recombining (3) and (4) in

$$\begin{cases} p^{\text{ap},\varepsilon}(0^-, x_2) = \varepsilon\mathcal{A}\frac{\partial p^{\text{ap},\varepsilon}}{\partial x_1}(0^+, x_2) - \varepsilon\mathcal{B}\frac{\partial p^{\text{ap},\varepsilon}}{\partial x_1}(0^-, x_2), \\ p^{\text{ap},\varepsilon}(0^+, x_2) = \varepsilon\mathcal{B}\frac{\partial p^{\text{ap},\varepsilon}}{\partial x_1}(0^+, x_2) - \varepsilon\mathcal{A}\frac{\partial p^{\text{ap},\varepsilon}}{\partial x_1}(0^-, x_2). \end{cases} \quad (7)$$

Obviously $p^{\text{ap},\varepsilon} = p_0 + \varepsilon p_1 + O(\varepsilon^2)$; hence both $p^{\text{ap},\varepsilon}$ and $(p_0 + \varepsilon p_1)$ approximate p up to $O(\varepsilon^2)$.

Remark 2.1 *The above relations are written in the case of wires being symmetric with respect to y_1 ; otherwise an additional elementary solution Q^- is involved resulting in an additional constant, see (2.31) in [10]. The elementary solution Q^- is the 1-periodic w.r.t. to y_2 solution to*

$$\Delta Q^- = 0, \quad \text{in } \Upsilon, \quad Q^- = 0 \quad \text{on } \partial\hat{\Upsilon}, \quad \text{and } \lim_{y_1 \rightarrow -\infty} \nabla Q^- = \mathbf{e}_1, \quad \lim_{y_1 \rightarrow +\infty} \nabla Q^- = \mathbf{0}. \quad (8)$$

For symmetric wires, $Q^-(y_1, y_2) = -Q^+(-y_1, y_2)$ hence $Q^- \underset{y_1 \rightarrow -\infty}{\sim} y_1 - \mathcal{B}$ and $Q^- \underset{y_1 \rightarrow +\infty}{\sim} -\mathcal{A}$.

2.2 Remark on a simple scattering problem

Let us stress a drawback of an iterative resolution when illuminating the array by an incident wave e^{-ikx_1} (coming from $+\infty$) at normal incidence on the array, hence a solution of the form

$$p^{\text{ap}}(\mathbf{x}) = e^{-ikx_1} + \mathcal{R}^{\text{ap}}e^{ikx_1} \quad \text{for } x_1 > 0, \quad p^{\text{ap}}(\mathbf{x}) = \mathcal{T}^{\text{ap}}e^{-ikx_1} \quad \text{for } x_1 < 0. \quad (9)$$

In an iterative resolution, \mathcal{R}^{ap} is sought of the form $\mathcal{R}^{\text{ap}} = \mathcal{R}_0 + \varepsilon\mathcal{R}_1$ up to the first order (the same for \mathcal{T}^{ap}). The solution p_0 ruled by (3) provides $\mathcal{R}_0 = -1$ and $\mathcal{T}_0 = 0$. Next p_1 , of the form $\mathcal{R}_1e^{ikx_1}$ for $x_1 > 0$ and $\mathcal{T}_1e^{-ikx_1}$ for $x_1 < 0$, and ruled by (4) provides $\mathcal{R}_1 = -2ikh\mathcal{B}$ and $\mathcal{T}_1 = -2ikh\mathcal{A}$. Reconstructing \mathcal{R}^{ap} and \mathcal{T}^{ap} up to the first order leads to

$$\mathcal{R}^{\text{ap}} = (\mathcal{R}_0 + \varepsilon\mathcal{R}_1) = -(1 + 2ikh\mathcal{B}), \quad \mathcal{T}^{\text{ap}} = (\mathcal{T}_0 + \varepsilon\mathcal{T}_1) = -2ikh\mathcal{A}, \quad (10)$$

which do not satisfied the conservation of the fluxes $|\mathcal{R}^{\text{ap}}|^2 + |\mathcal{T}^{\text{ap}}|^2 = 1$. (They satisfy the conservation up to $O(\varepsilon^2)$). Consider now the solution (9)

ruled by the unified conditions (7), we obtain

$$\mathcal{R}^{\text{ap}} = -\frac{1 - (kh)^2(\mathcal{A}^2 - \mathcal{B}^2)}{1 - 2ikh\mathcal{B} + (kh)^2(\mathcal{A}^2 - \mathcal{B}^2)}, \quad \mathcal{T}^{\text{ap}} = \frac{-2ikh\mathcal{A}}{1 - 2ikh\mathcal{B} + (kh)^2(\mathcal{A}^2 - \mathcal{B}^2)}, \quad (11)$$

which satisfies exactly $|\mathcal{R}^{\text{ap}}|^2 + |\mathcal{T}^{\text{ap}}|^2 = 1$. By construction, $(\mathcal{R}_0 + \varepsilon\mathcal{R}_1)$ and $(\mathcal{T}_0 + \varepsilon\mathcal{T}_1)$ in (10) are the expansions up to $O(\varepsilon^2)$ of \mathcal{R}^{ap} and \mathcal{T}^{ap} in (11). We may say that (11) contains non valuable terms $O(\varepsilon^2)$; this has no consequence. To the opposite, cancelling these terms *a posteriori* would affect the properties of the solution, here the conservation of the fluxes. We can say as a rule that the solutions of the unified problem do not have to be interrogated again.

3 A linear array atop a Dirichlet wall (a cage)

We now envision a Faraday cage, see figure 2. We consider two rectangular domains $\Omega^+ = (0, d^+) \times (0, \ell)$ and $\Omega^- = (-d^-, 0) \times (0, \ell)$, with $d^\pm, \ell > 0$, that share the common interface $\Gamma = \{(0, x_2) \in \mathbb{R}^2, x_2 \in (0, \ell)\}$. We denote by $\Omega = \Omega^+ \cup \Omega^- \cup \Gamma$ and by Γ^\pm the lateral boundaries of Ω , *i.e.*

$$\Gamma^\pm = \{(\pm d^\pm, x_2) \in \mathbb{R}^2, x_2 \in (0, \ell)\}.$$

A large positive integer $N > 0$ is the number of wires in $(0, \ell)$, whence $N \sim \frac{\ell}{\varepsilon}$, and the analysis holds far from the lateral boundaries at $x_2 = 0, 1$. We puncture the domain Ω along the interface Γ by subtracting the set $\mathcal{L}^\varepsilon = \bigcup_{1 \leq i \leq N} \varepsilon \{\bar{\mathcal{Y}} + i\mathbf{e}_2\}$. Finally, our domain is the open set $\Omega^\varepsilon = \Omega \setminus \mathcal{L}^\varepsilon$. On that domain, we consider the Helmholtz equation written in non-dimensional form with $K = (kL)^2$: find p^ε solution to

$$\begin{cases} \Delta p^\varepsilon + Kp^\varepsilon = S, & \text{in } \Omega^\varepsilon, \\ \partial_n p^\varepsilon = i\sqrt{K}p^\varepsilon & \text{on } \Gamma^+, \quad p^\varepsilon = 0 & \text{on } \partial\Omega^\varepsilon \setminus \Gamma^+, \end{cases} \quad (12)$$

where S is a source term compactly supported in Ω^+ (figure 2). Providing S is regular enough, Problem (12) is well-posed.

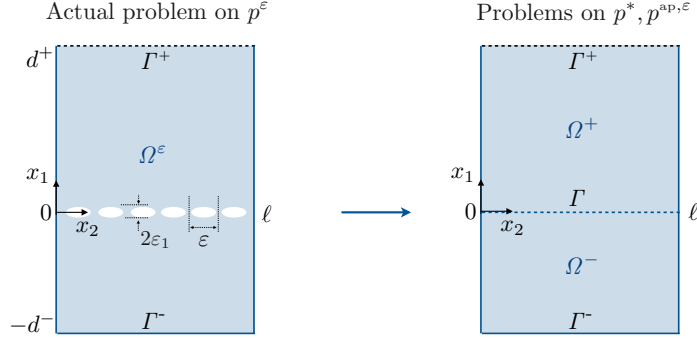


Figure 2: A linear array atop a Dirichlet wall Γ^- – The actual problem (12) on p^ε and as results of asymptotic analysis, the limit problem (13) on p^* and of the unified problem (14) on $p^{\text{ap},\varepsilon}$.

3.1 The question put to the unified problem

As $\varepsilon \rightarrow 0$, Problem (12) “tends” to the following limit problem: find p^* solution to

$$\begin{cases} \Delta p^* + K p^* = S & \text{in } \Omega^+, \\ \partial_n p^* = i\sqrt{K} p^* & \text{on } \Gamma^+, \quad p^* = 0 & \text{on } \partial\Omega^+ \setminus \Gamma^+, \end{cases} \quad \begin{cases} \Delta p^* + K p^* = 0 & \text{in } \Omega^-, \\ p^* = 0 & \text{on } \partial\Omega^-, \end{cases} \quad (13)$$

and it turns out that the limit problem uncouples the behavior of p^* above and below Γ . (The limit problem is the zero-order problem, $p^* = p_0$, involving the boundary condition (3).) As previously said, Problem (13-right) that is posed in Ω^- may be ill-posed while the initial problem is not. Indeed, there exists a sequence of values $(K_n^*)_{n \in \mathbb{N}}$ where Problem (13-right) admits a non trivial kernel of finite dimension. These values are known as the eigenvalues of the Laplace operator in Ω^- with Dirichlet boundary conditions which are the perfect resonances of the closed cavity Ω^- . This ill-posed limit problem reflects the presence of the quasi-resonances for the actual problem (12) having a small imaginary part due to radiative damping and a real part close to K_n^* .

Away from these particular frequencies, we expect that the unified up-to-first-order problem (7) can be used. Specifically, p^ε can be approximated (with

an error of order ε^2) by solving the following problem: find $p^{\text{ap},\varepsilon}$ solution to

$$\left\{ \begin{array}{ll} \Delta p^{\text{ap},\varepsilon} + K p^{\text{ap},\varepsilon} = S & \text{in } \Omega^+, & \Delta p^{\text{ap},\varepsilon} + K p^{\text{ap},\varepsilon} = S & \text{in } \Omega^-, \\ \frac{\partial p^{\text{ap},\varepsilon}}{\partial x_1} = i\sqrt{K} p^{\text{ap},\varepsilon} & \text{on } \Gamma^+, & p^{\text{ap},\varepsilon} = 0 & \text{on } \partial\Omega^- \setminus \Gamma, \\ p^{\text{ap},\varepsilon} = 0 & \text{on } \partial\Omega^+ \setminus (\Gamma \cup \Gamma^+), & & \\ p^{\text{ap},\varepsilon}_{|0^+} = \varepsilon \mathcal{B} \frac{\partial p^{\text{ap},\varepsilon}}{\partial x_1}_{|0^+} - \varepsilon \mathcal{A} \frac{\partial p^{\text{ap},\varepsilon}}{\partial x_1}_{|0^-}, & & p^{\text{ap},\varepsilon}_{|0^-} = \varepsilon \mathcal{A} \frac{\partial p^{\text{ap},\varepsilon}}{\partial x_1}_{|0^+} - \varepsilon \mathcal{B} \frac{\partial p^{\text{ap},\varepsilon}}{\partial x_1}_{|0^-} & \text{on } \Gamma. \end{array} \right. \quad (14)$$

We emphasize that, unlike the limit problem (13), Problem (14) turns out to be well-posed for any dimensionless frequency K . However this does not presume that it approximates p^ε when K is close to an eigenvalue K_n^* of the limit problem (13-right). This is the question addressed in the rest of this section. To do so, we consider K_n^* a simple eigenfrequency of the cavity problem (13-right) and the resonance frequency K_n of the actual cavity is close to that eigenfrequency. Being "far from" or "close to" the resonance can be measured by the relative amplitudes of the fields p^ε inside and outside the cavity. Outside the cavity, $p^\varepsilon = O(1)$ imposed by the source, and we define three cases :

- *The off-resonance case (1)* – It corresponds to $|K - K_n^*| = O(1)$, hence far from the perfect resonance, and we shall see that $p^\varepsilon = O(\varepsilon)$ is small within the cavity Ω^- . This is the case where the validity of (14) is not really questioned.
- *The near-resonance (2i) and on-resonance case (2ii)* – These cases correspond to K close to K_n^* with

$$K(\varepsilon) = K_n^* + \varepsilon \kappa_1 + \varepsilon^2 \kappa_2, \quad (15)$$

(see figure 3). For an arbitrary κ_1 , $p^\varepsilon = O(1)$ becomes significant within the cavity Ω^- ; it is termed the near-resonance (2i). Arbitrary κ_1 means $\kappa_1 \neq \kappa$, κ being a specific value which makes $(K_n^* + \varepsilon \kappa)$ close to the actual resonance K_n , see forthcoming (20). This on-resonance case (2ii) is characterized by large amplitudes $p^\varepsilon = O(\frac{1}{\varepsilon})$ inside the cavity. In this close vicinity of the actual resonance $|K - K_n^* - \varepsilon \kappa| = O(\varepsilon^2)$, the parameter κ_2 can be used to get the resonance curve as $\alpha_2(\kappa_2) = \varepsilon \sqrt{\int_{\Omega^-} |p^\varepsilon|^2}$.

The performance of Problem (14) to approximate p^ε in the cases (1), (2i) and (2ii) is demonstrated below. The demonstration relies on the construction of asymptotic expansions of p^ε and $p^{\text{ap},\varepsilon}$ and we shall see that the leading orders of the two expansions coincide in the three cases. This was expected,

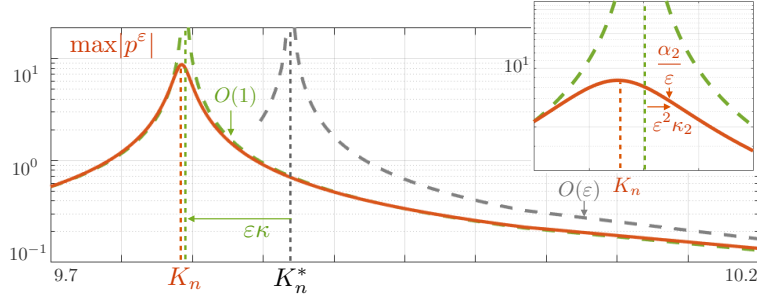


Figure 3: Resonance curve by means of $\max|p^\varepsilon|$ in the cavity Ω^ε close to the resonance K_n (plain red line). The dashed grey line shows the off-resonance solution blowing up at the resonance K_n^* of the close cavity (its validity is limited to $p^\varepsilon = O(\varepsilon)$). The dashed green line shows the near-resonance solution blowing up at $(K_n^* + \varepsilon\kappa)$ close to the actual resonance K_n (its validity is limited to $p^\varepsilon = O(1)$). The inset shows the parametrization of the resonance curve in the on-resonance regime whose validity is limited to $p^\varepsilon = O(\frac{1}{\varepsilon})$.

by construction, in the case (1) but it may appear surprising in the resonant cases (2).

Remark 3.1 *We restrict ourselves to the case where K_n^* is a simple eigenfrequency of the cavity problem (13-right). The result holds for multiple eigenfrequencies but requires more involved calculations.*

3.2 Asymptotic behaviour of the exact solution

The determination of the asymptotic behaviour of p^ε is based on the method of matched asymptotic expansions, which permits to capture the boundary layer effect occurring in the vicinity of the wires. The main idea is to distinguish between two "far field regions" located far from Γ and a near field area located in its vicinity, the two types of expansions matching in some intermediate area. In the present case, we can construct asymptotic expansions of the form

$$p^\varepsilon = \begin{cases} \sum_{m \geq m_0} \varepsilon^m p_m(x_1, x_2) & \text{far from } \Gamma \quad (\text{far field expansion}), \\ \sum_{m \geq m_0} \varepsilon^m q_m\left(\frac{x_1}{\varepsilon}, \frac{x_2}{\varepsilon}, x_2\right) & \text{in the vicinity of } \Gamma \quad (\text{near field expansion}), \end{cases} \quad (16)$$

where the integer m_0 will be equal to -1 or 0 . Since we are interested in the macroscopic behavior of p^ε , we present the results on the leading order

in the far field expansion; the step-by-step construction of the asymptotic expansion is technical and it is postponed in Appendix A.

3.2.1 The off-resonance case (1)

The off-resonance case consists in taking a fixed $K \neq K_n^*$ (independent of ε) that is not an eigenvalue of the cavity problem (13-left).

Lemma 3.2 *Assume that K is not an eigenvalue of the cavity problem (13-left). Then, far from Γ , p^ε admits the following leading-order asymptotic*

$$p^\varepsilon \sim \begin{cases} P^* & \text{in } \Omega^+, \\ \varepsilon \mathcal{A}p^- & \text{in } \Omega^-, \end{cases} \quad (17)$$

where P^* is the unique solution to (13-left) and p^- is the unique solution to

$$\begin{cases} \Delta p^- + Kp^- = 0 & \text{in } \Omega^-, \\ p^- = 0 & \text{on } \partial\Omega^- \setminus \Gamma, \quad p^- = \frac{\partial P^*}{\partial x_1} & \text{on } \Gamma, \end{cases} \quad (18)$$

We point out that $p^\varepsilon = \varepsilon \mathcal{A}p^-$ is small in the cavity Ω^- , which means that the array efficiently shields the domain Ω^- .

3.2.2 The near-resonance case (2i): $\kappa_1 \neq \kappa$

We consider K_n^* a simple eigenfrequency of the cavity problem (13-right), which is for instance the case for the first eigenvalue in two dimensions. We denote by p_n^* a corresponding real-valued eigenvector such that

$$\int_{\Omega^-} (p_n^*)^2 d\mathbf{x} = 1. \quad (19)$$

Remark 3.3 *Obviously the orthogonality condition (19) does not entirely define p_n^* among all the normalized eigenvectors associated with the eigenvalue K_n^* . Indeed if p_n^* fulfills (19), so does $-p_n^*$. Naturally the arbitrary choice of p_n^* does not change the results below.*

Then, we take $K(\varepsilon)$ of the form (15) which means that we consider frequencies located in a ε -neighborhood of K_n^* . At that stage, we introduce the real number κ

$$\kappa = -\mathcal{B} \int_{\Gamma} \left(\frac{\partial p_n^*}{\partial x_1}(0, x_2) \right)^2 dx_2, \quad (20)$$

with \mathcal{B} the constant appearing in (14). We shall make the distinction between the two sub-cases (2i) $\kappa_1 \neq \kappa$ and (2ii) $\kappa_1 = \kappa$, and we start here with $\kappa_1 \neq \kappa$.

Lemma 3.4 Assume that K is of the form (15) and that $\kappa_1 \neq \kappa$. Then, far from Γ , p^ε admits the following behavior

$$p^\varepsilon \sim \begin{cases} P_n^*, & \text{in } \Omega^+, \\ \alpha_1 p_n^*, & \text{in } \Omega^-, \end{cases} \quad \text{with} \quad \alpha_1 = \frac{\mathcal{A}I}{\kappa_1 - \kappa}, \quad (21)$$

where P_n^* is the unique solution to (13-left) for $K = K_n^*$, \mathcal{A} is the constant appearing in (14) and

$$I = \int_{\Gamma} \frac{\partial P_n^*}{\partial x_1}(0, x_2) \frac{\partial p_n^*}{\partial x_1}(0, x_2) dx_2. \quad (22)$$

By contrast to the non-resonant case, $p^\varepsilon = \alpha_1 p_n^*$ is of order unity inside the cavity. There is no shielding effect as the fields are as intense inside and outside the cavity.

3.2.3 The resonant case (2ii): $\kappa_1 = \kappa$

Lemma 3.5 Assume that K is of the form (15) and that $\kappa_1 = \kappa$. Then p^ε has the following behavior

$$p^\varepsilon \sim \begin{cases} P_n^* + \alpha_2 \mathcal{A}P^+ & \text{in } \Omega^+, \\ \frac{\alpha_2}{\varepsilon} p_n^*, & \text{in } \Omega^-, \end{cases} \quad \text{with} \quad \alpha_2 = \frac{\mathcal{A}I}{\kappa_2 - \mathcal{A}^2 I^+ + \mathcal{B}^2 I^-}, \quad (23)$$

with I is defined in (22), I^\pm are defined by

$$I^+ = \int_{\Gamma} \frac{\partial P^+}{\partial x_1}(0, x_2) \frac{\partial p_n^*}{\partial x_1}(0, x_2) dx_2, \quad I^- = \int_{\Gamma} \frac{\partial P^-}{\partial x_1}(0, x_2) \frac{\partial p_n^*}{\partial x_1}(0, x_2) dx_2, \quad (24)$$

and P^+ and P^- are the (unique) solutions to

$$\begin{cases} \Delta P^+ + K_n^* P^+ = 0 & \text{in } \Omega^+, \\ \frac{\partial P^+}{\partial x_1} = i\sqrt{K_n^*} P^+ & \text{on } \Gamma^+, \\ P^+ = -\frac{\partial p_n^*}{\partial x_1} & \text{on } \Gamma, \\ P^+ = 0 & \text{on } \partial\Omega^+ \setminus (\Gamma^+ \cup \Gamma) \end{cases} \quad \begin{cases} \Delta P^- + K_n^* P^- = -\frac{\kappa}{\mathcal{B}} p_n^*, & \text{in } \Omega^-, \\ P^- = 0 & \text{on } \partial\Omega^- \setminus \Gamma, \\ P^- = -\frac{\partial p_n^*}{\partial x_1} & \text{on } \Gamma, \\ \int_{\Omega^-} P^- p_n^* d\mathbf{x} = 0. \end{cases} \quad (25)$$

In the close vicinity of a resonance, the field $p^\varepsilon = O(\frac{1}{\varepsilon})$ in Ω^- becomes more intense within the cavity than outside and it would blow up as ε vanishes. Indeed, in the limit of zero ε , p^ε tends to p^* and we recover a perfect resonance with unbounded amplitude inside the cavity.

3.3 Asymptotic behaviours of the homogenized solution

The obtention of the asymptotic behaviour of $p^{\text{ap},\varepsilon}$ solution to (14) also relies on the construction of its asymptotic expansion. However, this expansion is much simpler than that of p^ε . Indeed, the approximate problem does not see the wires and we have a classical expansion of the form

$$p^{\text{ap},\varepsilon} = \sum_{m \geq m_0} \varepsilon^m p_m^{\text{ap}}(x_1, x_2) \quad \text{in } \Omega^+ \cup \Omega^-, \quad (26)$$

where m_0 is equal to -1 or 0 . Below we show that we recover the off-resonance (17) and the two different resonant cases-(21) and (23), corresponding to (15).

3.3.1 The off-resonance case

In that case, as for the exact problem, the formal expansion (26) is plugged into (14), and we find $m_0 = 0$ ($p_{-1}^{\text{ap}} = 0$ in Ω^+ and Ω^-). Next, p_0^{ap} is solution to

$$\begin{cases} \Delta p_0^{\text{ap}} + K p_0^{\text{ap}} = S & \text{in } \Omega^+, \\ \frac{\partial p_0^{\text{ap}}}{\partial x_1} = i\sqrt{K} p_0^{\text{ap}} & \text{on } \Gamma^+, \quad p_0^{\text{ap}} = 0 \quad \text{on } \partial\Omega^+ \setminus \Gamma^+, \end{cases} \quad \begin{cases} \Delta p_0^{\text{ap}} + K p_0^{\text{ap}} = 0 & \text{in } \Omega^-, \\ p_0^{\text{ap}} = 0 & \text{on } \partial\Omega^-, \end{cases} \quad (27)$$

and as $K \neq K_n^*$ the solution reads

$$p_0^{\text{ap}} = \begin{cases} P^* & \text{in } \Omega^+, \\ 0 & \text{in } \Omega^-. \end{cases}$$

In Ω^- , the first non-zero contribution appears at the order 1, with p_1^{ap} solution to

$$\begin{cases} \Delta p_1^{\text{ap}} + K p_1^{\text{ap}} = 0 & \text{in } \Omega^-, \\ p_1^{\text{ap}} = 0 \quad \text{on } \partial\Omega^- \setminus \Gamma, \quad p_1^{\text{ap}} = \mathcal{A} \frac{\partial P^*}{\partial x_1}, & \text{on } \Gamma. \end{cases}$$

Remembering that we have denoted p^- the unique solution to (18), we obtain that $p_1^{\text{ap}} = \mathcal{A} p^-$. Eventually, we get for $p^{\text{ap},\varepsilon} = p_0^{\text{ap}} + \varepsilon p_1^{\text{ap}} + O(\varepsilon^2)$ the leading-order asymptotic

$$p^{\text{ap},\varepsilon} \sim \begin{cases} P^* & \text{in } \Omega^+, \\ \varepsilon \mathcal{A} p^- & \text{in } \Omega^-, \end{cases}$$

which coincides with (17).

3.3.2 The near-resonance case $\kappa_1 \neq \kappa$

In that case, inserting the formal expansion into (14) and separating the different powers of ε , we find again that $m_0 = 0$. But now, p_0^{ap} is solution to

$$\begin{cases} \Delta p_0^{\text{ap}} + K_n^* p_0^{\text{ap}} = S & \text{in } \Omega^+, \\ \frac{\partial p_0^{\text{ap}}}{\partial x_1} = i\sqrt{K_n^*} p_0^{\text{ap}} & \text{on } \Gamma^+, \quad p_0^{\text{ap}} = 0 \quad \text{on } \partial\Omega^+ \setminus \Gamma^+, \end{cases} \quad \begin{cases} \Delta p_0^{\text{ap}} + K_n^* p_0^{\text{ap}} = 0 & \text{in } \Omega^-, \\ p_0^{\text{ap}} = 0 & \text{on } \partial\Omega^-. \end{cases} \quad (28)$$

The problem (28-left) is identical to (27-left) for $K = K_n^*$ and we have denoted P_n^* its unique solution. In contrast, the problem (28-right) is ill-posed at the eigenfrequency K_n^* of the close cavity. However, as p_n^* is the eigenvector associated with K_n^* , we can write

$$p_0^{\text{ap}} = \begin{cases} P_n^* & \text{in } \Omega^+, \\ \alpha_1^{\text{ap}} p_n^* & \text{in } \Omega^-, \end{cases}$$

but α_1^{ap} is unknown. (This means that the problem at the dominant first order cannot be solved; it corresponds to the limit problem (13) at an eigenvalue of the Laplace operator in Ω^- .) The value of α_1^{ap} is obtained from the first-order problem in Ω^- , namely find p_1^{ap} solution to

$$\begin{cases} \Delta p_1^{\text{ap}} + K_n^* p_1^{\text{ap}} = -\kappa_1 \alpha_1^{\text{ap}} p_n^* & \text{in } \Omega^-, \\ p_1^{\text{ap}} = \mathcal{A} \frac{\partial P_n^*}{\partial x_1} - \mathcal{B} \alpha_1^{\text{ap}} \frac{\partial p_n^*}{\partial x_1} & \text{on } \Gamma, \quad p_1^{\text{ap}} = 0 \quad \text{on } \partial\Omega^- \setminus \Gamma, \end{cases}$$

which is solvable if and only if

$$\alpha_1^{\text{ap}} = \frac{\mathcal{A}}{\kappa_1 - \kappa} \int_{\Gamma} \frac{\partial P_n^*}{\partial x_1}(0, x_2) \frac{\partial p_n^*}{\partial x_1}(0, x_2) dx_2,$$

(making use of (19) and (20)) and we exactly recover (21) (with $\alpha_1^{\text{ap}} = \alpha_1$).

3.3.3 The on-resonance case $\kappa_1 = \kappa$

Inserting the formal expansion (26) into (14), we find $m_0 = -1$ with p_{-1}^{ap} solution to

$$\begin{cases} \Delta p_{-1}^{\text{ap}} + K_n^* p_{-1}^{\text{ap}} = 0 & \text{in } \Omega^+, \\ \frac{\partial p_{-1}^{\text{ap}}}{\partial x_1} = i\sqrt{K_n^*} p_{-1}^{\text{ap}} & \text{on } \Gamma^+, \quad p_{-1}^{\text{ap}} = 0 \quad \text{on } \partial\Omega^+ \setminus \Gamma^+, \end{cases} \quad \begin{cases} \Delta p_{-1}^{\text{ap}} + K_n^* p_{-1}^{\text{ap}} = 0 & \text{in } \Omega^-, \\ p_{-1}^{\text{ap}} = 0 & \text{on } \partial\Omega^-. \end{cases}$$

The term p_{-1}^{ap} plays basically the same role as p_0^{ap} in the near-resonance case. It is solution to (27-left) in Ω^+ but without the source S hence $p_{-1}^{\text{ap}} = 0$ in Ω^+ . It is solution to the ill-posed problem (28-right) in Ω^- hence equal to p_n^* up to an unknown constant α_2^{ap} in Ω^- , namely

$$p_{-1}^{\text{ap}} = \begin{cases} 0, & \text{in } \Omega^+, \\ \alpha_2^{\text{ap}} p_n^*, & \text{in } \Omega^-. \end{cases}$$

As in the near-resonant case, α_2^{ap} is obtained from the problem at the next order, in the present case, the zero order. At the zero order, p_0^{ap} is solution to

$$\begin{cases} \Delta p_0^{\text{ap}} + K_n^* p_0^{\text{ap}} = S & \text{in } \Omega^+, \\ \frac{\partial p_0^{\text{ap}}}{\partial x_1} = i\sqrt{K_n^*} p_0^{\text{ap}} & \text{on } \Gamma^+, \quad p_0^{\text{ap}} = 0, \quad \text{on } \partial\Omega^+ \setminus (\Gamma^+ \cup \Gamma), \\ p_0^{\text{ap}} = -\mathcal{A} \alpha_2^{\text{ap}} \frac{\partial p_n^*}{\partial x_1} & \text{on } \Gamma, \end{cases} \quad \begin{cases} \Delta p_0^{\text{ap}} + K_n^* p_0^{\text{ap}} = -\kappa \alpha_2^{\text{ap}} p_n^* & \text{in } \Omega^-, \\ p_0^{\text{ap}} = 0 & \text{on } \partial\Omega^- \setminus \Gamma, \\ p_0^{\text{ap}} = -\mathcal{B} \alpha_2^{\text{ap}} \frac{\partial p_n^*}{\partial x_1} & \text{on } \Gamma. \end{cases}$$

As P^+ is solution to (25-left) and P_n^* is solution to (13-left) for $K = K_n^*$, we recover that

$$p_0^{\text{ap}} = \alpha_2^{\text{ap}} \mathcal{A} P^+ + P_n^* \quad \text{in } \Omega^+,$$

as in (23), but α_2^{ap} has to be determined. Besides, the problem in Ω^- is solvable by construction (with $\kappa_1 = \kappa$) and with P^- solution to (25-right) we have

$$p_0^{\text{ap}} = \alpha_2^{\text{ap}} \mathcal{B} P^- + \beta^{\text{ap}} p_n^* \quad \text{in } \Omega^-,$$

where β^{ap} is unknown at this order (but we do not need to determine it). As we have done to find α_1^{ap} in the near-resonance case, we determine the value of α_2^{ap} using the solvability condition for p_1^{ap} in Ω^- , solution to

$$\begin{cases} \Delta p_1^{\text{ap}} + K_n^* p_1^{\text{ap}} = -\kappa_1 (\alpha_2^{\text{ap}} \mathcal{B} P^- + \beta_*^{\text{ap}} p_n^*) - \kappa_2 \alpha_2^{\text{ap}} p_n^* & \text{in } \Omega^-, \\ p_1^{\text{ap}} = 0 & \text{on } \Omega^- \setminus \Gamma, \quad p_1^{\text{ap}} = \mathcal{A} \left(\alpha_1^{\text{ap}} \mathcal{A} \frac{\partial P^+}{\partial x_1} + \frac{\partial P_n^*}{\partial x_1} \right) - \mathcal{B} \left(\alpha_2^{\text{ap}} \frac{\partial P^-}{\partial x_1} + \beta_*^{\text{ap}} \frac{\partial p_n^*}{\partial x_1} \right) & \text{on } \Gamma, \end{cases}$$

and we get that $\alpha_2^{\text{ap}} = \frac{\mathcal{A}I}{\kappa_2 - \mathcal{A}^2 I^+ + \mathcal{B}^2 I^-}$, hence we entirely recover (23) ($\alpha_2^{\text{ap}} = \alpha_2$).

4 A one-dimensional cage in the harmonic regime

To begin with, we consider a one-dimensional cage which means a cage laterally unbounded along x_2 . In the harmonic regime, the time dependence is

$e^{-i\omega t}$ and the scattering problem is set for an incident wave with wavenumber $\mathbf{k} = k(c_\theta, s_\theta)$, $c_\theta^2 + s_\theta^2 = 1$ and $k = \frac{\omega}{c}$ (we use $c = 1$). The wave comes from $x_1 = +\infty$ on the array, hence pseudo-periodic conditions along x_2 apply. The array is made of square wires $e = e_1 = e_2$ and spacing $h = 1$ (with arbitrary unit) at distance $D = 7$ of a Dirichlet wall Γ^- . We call p the solution of the actual problem computed numerically using a modal method described in [10]; we call p^{ap} (omitting ε) the solution of the homogenized problem.

4.1 Validity of the unified model, comparison with the iterative model

4.1.1 Solution of the unified model

The solution of the scattering problem is explicit using (2) along with (7)¹. It reads $p^{\text{ap}}(\mathbf{x}) = p^{\text{ap}}(x_1)e^{iks_\theta x_2}$ with

$$p^{\text{ap}}(x_1) = \begin{cases} e^{-ikc_\theta x_1} + \mathcal{R}^{\text{ap}}e^{ikc_\theta x_1}, & \text{for } x_1 \in (0, +\infty), \\ \mathcal{P}^{\text{ap}} \sin(kc_\theta(x_1 + D)), & \text{for } x_1 \in (-D, 0), \end{cases} \quad (29)$$

and

$$\begin{cases} \mathcal{R}^{\text{ap}} = -\frac{\bar{z}}{z}, & \mathcal{P}^{\text{ap}} = -\frac{2ikc_\theta h \mathcal{A}}{z}, \\ \text{and } z = (1 - ikc_\theta h \mathcal{B}) \sin(kc_\theta D) + kc_\theta h (\mathcal{B} + ikc_\theta h (\mathcal{A}^2 - \mathcal{B}^2)) \cos(kc_\theta D). \end{cases} \quad (30)$$

Expectedly, $|\mathcal{R}^{\text{ap}}| = 1$ and \mathcal{P}^{ap} is bounded. Besides, defining the resonance as $\mathcal{R}^{\text{ap}} = 1$ provides the resonance frequency k_n and the corresponding amplitude $\mathcal{P}_{\text{max}}^{\text{ap}}$ by means of the condition that z is purely imaginary

$$\tan(k_n c_\theta D) + k_n c_\theta h \mathcal{B} = 0, \quad \mathcal{P}_{\text{max}}^{\text{ap}} = \frac{2}{\mathcal{A} k_n c_\theta h \cos(k_n c_\theta D)}, \quad (31)$$

hence $k_n c_\theta D \sim n\pi \left(1 - \frac{h\mathcal{B}}{D} + \left(\frac{h\mathcal{B}}{D}\right)^2\right)$. (We have checked that defining the resonances as the maximum amplitudes within the cavity provides almost the same results for $(k_n, \mathcal{P}_{\text{max}}^{\text{ap}})$.)

To begin with, we report in figure 4 the fields $p(\mathbf{x})$ and $p^{\text{ap}}(\mathbf{x})$ for 3 frequencies corresponding to the cases (1), (2i) and (2ii) studied in §3. Off-resonance, the incident wave is basically reflected as on a Dirichlet wall with

¹In dimensional form, ε is replaced by h in (7), since $\varepsilon \frac{\partial}{\partial x_1} = h \frac{\partial}{\partial x_1}$.

$\mathcal{R}^{\text{ap}} \simeq -1$ resulting in a weak amplitude within the cavity. In contrast, on-resonance $\mathcal{R}^{\text{ap}} \simeq 1$ and the amplitude is large within the cavity. In between, near-resonance, the fields inside and outside the cavity are comparable in amplitude. It is noticeable that the agreement between $p(\mathbf{x})$ and $p^{\text{ap}}(\mathbf{x})$ from (29) with (30) is qualitatively very good.

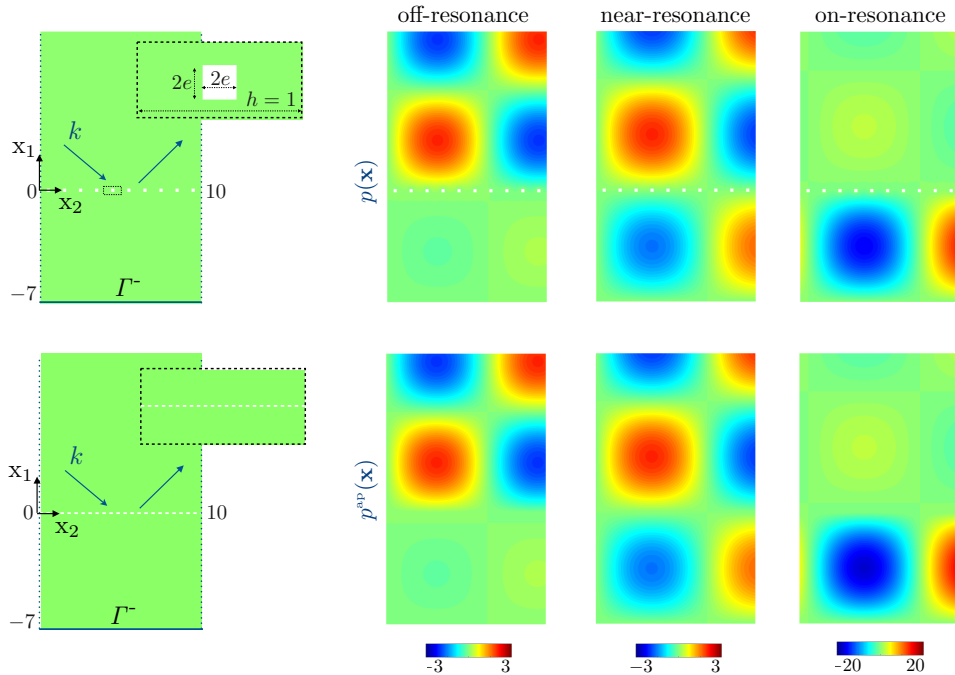


Figure 4: Wavefields in a 1D cage – $p(\mathbf{x})$ computed numerically and $p^{\text{ap}}(\mathbf{x})$ from (29)-(30). The source is a plane wave of amplitude unity at oblique incidence 45° on a periodic array of square wires with spacing $h = 1$ and with $e = e_1 = e_2 = 0.1$ ($x_2 \in (0, 10)$); the Dirichlet wall Γ is at $x_2 = -7$. The amplitude within the cavity is $O(\varepsilon)$ off-resonance ($k = 0.700$), $O(1)$ near-resonance ($k = 0.640$) and $O(\frac{1}{\varepsilon})$ on-resonance ($k = 0.633$).

The validity of (31) is further illustrated in figures 5 and 6. We have computed the maximum amplitude $\max|p|$ within the cavity against $k \in (0, 2)$ for $e = 0.01, 0.1$ and 0.2 (plain blue lines in figure 5). Next, $\max|p^{\text{ap}}|$, reported in dashed black lines, is determined from (29)-(30) (the values of $(\mathcal{A}, \mathcal{B})$ for $e = 0.01, 0.1$ and 0.2 are given in (56) in Appendix B). Notably, for $kc_\theta D > \frac{\pi}{2}$, we have $\max|p^{\text{ap}}| = \mathcal{P}^{\text{ap}}$. Classical trends of the resonance curves are observed. As e increases, the leakage of the cage decreases resulting in resonances with higher quality factors, that is thinner in frequency and higher in amplitude. These resonances take place close to $k_n^* c_\theta D = n\pi$, in the reported case $k_1^* = 0.635$, $k_2^* = 1.270$ and $k_3^* = 1.904$. The prediction of

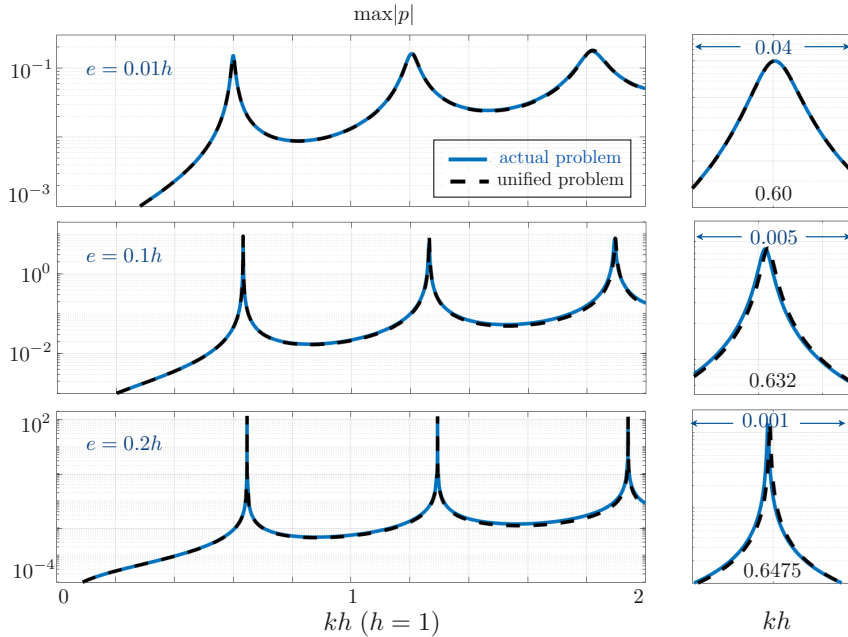


Figure 5: Maximum pressure in the cavity against the dimensionless frequency kh , $\max|p|$ from direct numerics (plain blue lines), $\max|p^{\text{ap},\varepsilon}|$ from (29)-(30) (dashed black lines). The right-panels show a zoom of the left-panels.

the unified problem appear to be excellent up to $kh = 2$ that is beyond the expected range of validity of the homogenisation (with $kh = O(\varepsilon)$ assumed to be small) although a slight discrepancy is visible above $kh \sim 1$ for $e = 0.1$ and 0.2 .

From the representation of figure 5, we have determined the resonance frequency k_1 and the corresponding amplitude at the resonance \mathcal{P}_{\max} against $h \in (0, 3)$. Results, in figure 6, show that the 1D cage has resonances behaving as for its 2D analog [7] and conform to (31). As the effective problem tends to the limit problem for vanishing h , decreasing h makes k_1 closer to k_1^* ; next k_1 departs from k_1^* essentially linearly with h . Amusingly, as in the 2D cage, $e \simeq 0.1h$ is a critical value; below k_1 decreases with h , above it increases. From (31), $k_n = k_n^*$ is obtained for $\mathcal{B} = 0$, and $\mathcal{B} = 0$ for $e \simeq 0.115h$. In any cases $\mathcal{P}_{\max} \sim \frac{1}{h}$ decreases with h as the leakage increases.

4.1.2 Comparison with the iterative model

The iterative model is made of 3 predictions, off-resonance, near-resonance and on-resonance. We have shown in §3 that the asymptotics of the unified

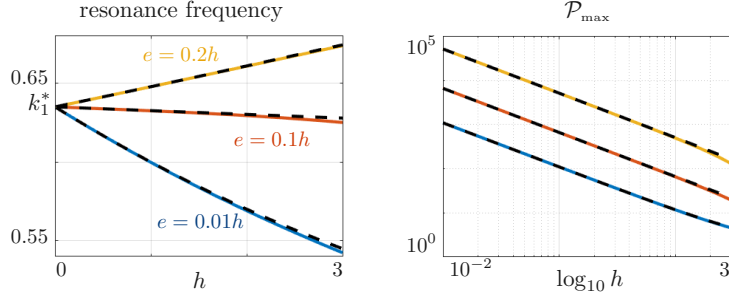


Figure 6: Variations of the resonance frequency k_1 and maximum amplitude \mathcal{P}_{\max} at the resonance against h . Plain lines: computed from direct numerics; dashed black lines: from (29).

model coincide with the iterative solution in the 3 regimes. However, this does not presume how the two solutions compare for a given h . As previously said, the problem is one-dimensional along x_1 which makes explicit the various functions needed to define the solutions of the iterative model, see ². We give below the resulting expressions in dimensional coordinate with $p^\varepsilon(x_1, x_2) = p^\varepsilon(x_1)e^{iks_\theta x_2}$.

• *Off-resonance case* – In this case $p^\varepsilon \sim \varepsilon \mathcal{A} p^-$ for $x_1 < 0$ (see (17)), hence using ², p^ε reads

$$p^\varepsilon(x_1) \sim \sum_{m=1}^{+\infty} \frac{-4i \frac{\mathcal{A}h}{D} \left(\frac{kc_\theta D}{m\pi}\right)^3 \sin\left(\frac{m\pi x_1}{D}\right)}{\left(\frac{kc_\theta D}{m\pi}\right)^2 - 1} - 2i \frac{\mathcal{A}h}{D} (kc_\theta D) \left(1 + \frac{x_1}{D}\right) \quad (32)$$

Expectedly, the amplitude within the cavity blows up at all the perfect resonances of the close cavity $kc_\theta D = m\pi$. (The solution is valid far from these resonances.)

Remark 4.1 *The solution (32) is the Taylor expansion of $p^{ap}(x_1)$ in (29) at*

²In non dimensional form and with $L = D$, hence $x_1 = \frac{x_1}{D} \in (-1, 0)$ ($\varepsilon = \frac{h}{D}$ and $K_n^* = (n\pi)^2$, $K = (kc_\theta D)^2$), we have

$$\left\{ \begin{array}{l} p^-(x_1) = - \sum_{m=1}^{+\infty} \frac{4iK^{3/2} \sin(m\pi x_1)}{m\pi(K - (m\pi)^2)} - 2i\sqrt{K}(1+x_1), P_n^*(x_1) = \sqrt{2} \sin(n\pi x_1), \quad P_n^*(x_1) = e^{-in\pi x_1} - e^{in\pi x_1}, \\ P^+(x_1) = -\sqrt{2}n\pi e^{in\pi x_1}, P^-(x_1) = -2\sqrt{2} \left(\sum_{m \neq n, m=1}^{+\infty} \frac{\frac{n}{m} \sin(m\pi x_1)}{1 - (\frac{m}{n})^2} + \sin(n\pi x_1) \right) - \sqrt{2}n\pi(1+x_1). \end{array} \right.$$

the first order in (kh) , hence $z \simeq \sin(kc_\theta D)$ in (30), see ³.

• *Near-resonance case* – From (21), $p^\varepsilon \sim \alpha_1 p_n^*$ for $x_1 < 0$ with $\alpha_1 = \frac{\mathcal{A}I}{\kappa_1 - \kappa}$ with $I = -2\sqrt{2}i(n\pi)^2$ and from (20), $\kappa = -2\mathcal{B}(n\pi)^2$ and $\kappa_1 = \frac{K - K_n^*}{\varepsilon} = \frac{D}{h}((kc_\theta D)^2 - (n\pi)^2)$, see ². Hence, we have

$$p^\varepsilon(x_1) \sim \frac{-4i \frac{\mathcal{A}h}{D} \sin\left(\frac{n\pi x_1}{D}\right)}{\left(\frac{kc_\theta D}{n\pi}\right)^2 - \left(1 - 2\frac{\mathcal{B}h}{D}\right)}. \quad (33)$$

Again, this amplitude blows up, but now at a value closer to the actual resonance frequency k_n , namely for $kc_\theta D \simeq n\pi \left(1 - \mathcal{B}\frac{h}{D}\right)$ corresponding to the first order expansion of the dispersion relation in (31). (The solution is valid far from this resonance.)

Remark 4.2 *The solution (33) coincides with the Taylor expansion of $p^{\text{ap}}(x_1)$ in (29) up to $O(\varepsilon^2)$, around the resonance of the close cavity, namely for $kc_\theta D = n\pi(1 + \varepsilon\hat{k})$ ⁴.*

• *On-resonance case* – Here, (23) applies, hence $p^\varepsilon \sim \frac{\alpha_2}{\varepsilon} p_n^*$ for $x_1 < 0$ with $\alpha_2 = \frac{\mathcal{A}I}{\kappa_2 - \mathcal{A}^2 I^+ + \mathcal{B}^2 I^-}$. Next, from (24) along with ², $I^+ = -2i(n\pi)^3$ and $I^- = -3(n\pi)^2$ (using ⁵) and by construction $\kappa_2 = \left(\frac{n\pi D}{h}\right)^2 \left[\left(\frac{kc_\theta D}{n\pi}\right)^2 - 1 + 2\frac{\mathcal{B}h}{D}\right]$. It follows that

$$p^\varepsilon(x_1) \sim \frac{-4i \frac{\mathcal{A}h}{D} \sin\left(\frac{n\pi x_1}{D}\right)}{\left(\frac{kc_\theta D}{n\pi}\right)^2 - \left(1 - 2\frac{\mathcal{B}h}{D} + 3\left(\frac{\mathcal{B}h}{D}\right)^2\right) + 2in\pi \left(\frac{\mathcal{A}h}{D}\right)^2}. \quad (34)$$

³The off-resonance case: (32) reads $p^\varepsilon(x_1) = \sum_{m=1}^{+\infty} \frac{-4i\varepsilon\mathcal{A}\left(\frac{\sqrt{K}}{m\pi}\right)^3 \sin(m\pi x_1)}{\left(\frac{\sqrt{K}}{m\pi}\right)^2 - 1} - 2i\varepsilon\mathcal{A}\sqrt{K}(1+x_1)$ in non-dimensional form, which coincides with $p^{\text{ap}}(x_1) = -\frac{2ikc_\theta h\mathcal{A}}{\sin(kc_\theta D)} \sin(kc_\theta(x_1 + D)) + O(\varepsilon^2)$ from (29)-(30) up to $O(\varepsilon^2)$, using $(1+x_1) = \sum_m \frac{-2}{m\pi} \sin(m\pi x_1)$ and $\sin(\sqrt{K}(x_1 + 1)) = \sum_m \frac{2m\pi \sin\sqrt{K}}{K - (m\pi)^2} \sin(m\pi x_1)$.

⁴The near-resonance case: (33) reads $p^\varepsilon(x_1) \sim \frac{-2i\mathcal{A}\sin(n\pi x_1)}{\hat{k} + \mathcal{B} + \frac{\varepsilon}{2}\hat{k}^2}$ which coincides with p^{ap} in (29) up to $O(\varepsilon)$, using that $\sin(\sqrt{K}(x_1 + 1)) = \cos(n\pi)\sin(n\pi x_1) + O(\varepsilon)$ and $\sin\sqrt{K} + \varepsilon\sqrt{K}(\cos\sqrt{K} - i\sin\sqrt{K}) = \varepsilon n\pi \cos(n\pi)(\hat{k} + \mathcal{B}) + O(\varepsilon^2)$.

⁵ for I^- we have used that $\sum_{m \neq n, m=1}^{+\infty} \frac{2}{1 - \left(\frac{m}{n}\right)^2} = -\frac{3}{2}$ for any n .

The leakage of the cavity is recovered hence the amplitude within the cavity is finite. This solution is valid in the close vicinity of the resonance k_n .

Remark 4.3 *Again, the solution (34) coincides with the Taylor expansion of $p^{\text{ap}}(x_1)$ in (29) up to $O(1)$, around the resonance $n\pi$ of the closed cavity $k c_\theta h = n\pi(1 - \varepsilon\mathcal{B} + \varepsilon^2\tilde{k})$ ⁶. We also obtain that the maximum amplitude is reached for*

$$(k_n c_\theta)^2 = \left(\frac{n\pi}{D}\right)^2 \left(1 - 2\frac{h\mathcal{B}}{D} + 3\left(\frac{h\mathcal{B}}{D}\right)^2\right),$$

which is the Taylor expansions of the dispersion relation in (31).

We end this comparison by reporting in figure 7 the same numerical result as in figure 5 but now we compare the actual solution with the solutions (32) (dashed grey lines) valid far from the resonances, (33) (dotted green lines)

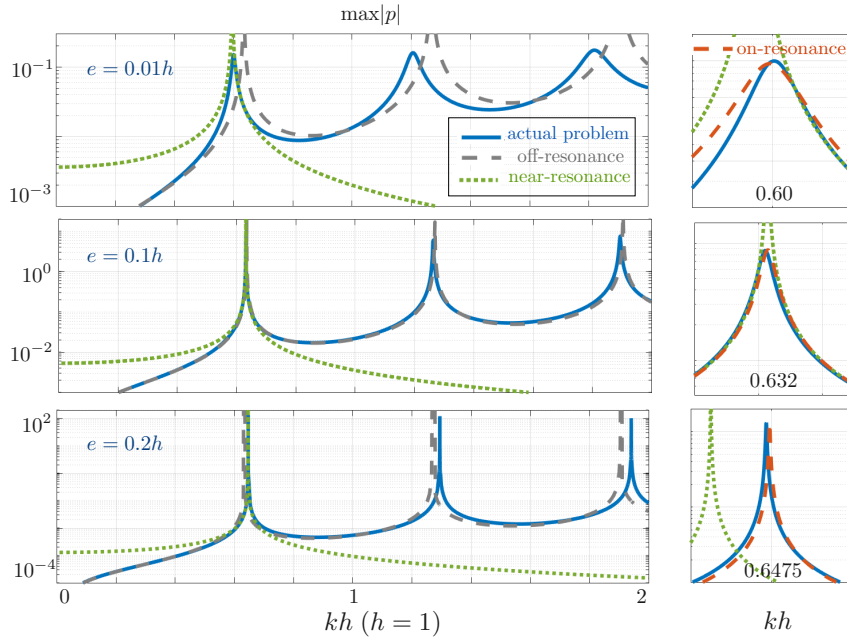


Figure 7: Same representation as in figure 5. Direct numerics for the actual problem and from the iterative model: off-resonance curve from (32), near-resonance curve from (33) and on-resonance curve from (34).

⁶The on-resonance case: In non-dimensional form (34) reads $p^\varepsilon(x_1) \sim \frac{-2i\mathcal{A}\sin(n\pi x_1)}{\varepsilon(\tilde{k} - \mathcal{B}^2 + in\pi\mathcal{A}^2 - \varepsilon\mathcal{B}\tilde{k} + \frac{\varepsilon^2}{2}\tilde{k}^2)}$, which has the same expansion up to $O(1)$ of p^{ap} in (29) which reads as $p^{\text{ap}}(x_1) = \frac{-2i\mathcal{A}\sin(n\pi x_1)}{\varepsilon(\tilde{k} - \mathcal{B}^2 + i(n\pi)\mathcal{A}^2)} + O(1)$.

valid near the first resonance and (34) (dashed red lines in the insets) in its close vicinity. The results are conform with those reported for the 2D cage in [7] and conform with the idea of piecewise-valid solutions. Compared to the unified solution which is valid in the whole range of frequency, the validity of each prediction is locally as good; the main difficulty in their use is to define the frequency ranges where each of them can be used. Eventually, it is visible that the result for $e = 0.01$ is not satisfactory essentially because the off-resonance solution departs significantly from the actual one; this case, which can be treated within the "thin wire approximation", is discussed in the Appendix C.

5 A two-dimensional cage in the transient regime

We now move on to the transient regime and consider a two-dimensional cage that is to say a cage laterally bounded along x_2 . As the fields depend on time and on space, we consider $p(\mathbf{x}) \rightarrow p(\mathbf{x}, t)$.

5.1 enlarged formulations of the model

To begin with, we note that the transmission conditions cannot be used as written in (7) that is written across a zero thickness interface. Introduced in [12, 13] enlarged formulations of the transmission conditions consist in modifying (7) by simple Taylor expansions of $p^{\text{ap}}(0^\pm, x_2, t)$ around $x_1 = \pm a$ with $a > 0$ resulting in (in dimensional form):

$$\begin{cases} p^{\text{ap}}(-a, x_2, t) = h\mathcal{A} \frac{\partial p^{\text{ap}}}{\partial x_1}(a, x_2, t) - (h\mathcal{B} + a) \frac{\partial p^{\text{ap}}}{\partial x_1}(-a, x_2, t), \\ p^{\text{ap}}(a, x_2, t) = (h\mathcal{B} + a) \frac{\partial p^{\text{ap}}}{\partial x_1}(a, x_2, t) - h\mathcal{A} \frac{\partial p^{\text{ap}}}{\partial x_1}(-a, x_2, t), \end{cases} \quad (35)$$

and we see that the new p^{ap} approximates p up to $O(\varepsilon^2)$ if $a = O(e_1) = O(h)$, see (B.9) in [11]. In other words, it exists a family of effective models parametrized by a and having the same asymptotic limit. The advantage of the models in enlarged formulations (35) is that they enjoy "good" energetic properties as soon as $a \geq a_c$ and we shall see that $0 \leq a_c \leq e_1$. For the time being, we show that it is sufficient that $a \geq e_1$: Let us consider the balance of energy in Ω be a bounded region of the space containing a segment Γ and $\Omega_a = \Omega \setminus \Gamma_a$ where $\Gamma_a = \{(x_1, x_2) \in (-a, a) \times \Gamma\}$ is the enlarged interface ruled by (35). Multiplying the first equation of (1) by \mathbf{u} , the second by p

and summing up, we get

$$\begin{cases} \frac{d}{dt}(\mathcal{E}^{\text{ap}} + \mathcal{E}_\Gamma) = 0, & \mathcal{E}^{\text{ap}}(t; a) = \frac{1}{2} \int_{\Omega_a} ((\mathbf{u}^{\text{ap}})^2 + (p^{\text{ap}})^2) \, d\mathbf{x}, \\ \mathcal{E}_\Gamma(t; a) = \frac{h}{2} \int_\Gamma \left(\left(\mathcal{B} + \frac{a}{h} \right) \left(u_{1|a}^{\text{ap}2} + u_{1|-a}^{\text{ap}2} \right) - 2\mathcal{A}u_{1|-a}^{\text{ap}}u_{1|a}^{\text{ap}} \right) \, dx_2. \end{cases} \quad (36)$$

($u_{1|\pm a}^{\text{ap}}$ stands for $u_1^{\text{ap}}(\pm a, x_2, t)$.) "Good" energetic properties means that the effective interface provides a positive energy contribution \mathcal{E}_Γ , a lack of which may lead to severe instability of any time-discretization scheme; this will be illustrated in the forthcoming §5.3.

Lemma 5.1 *The quadratic form $(\mathcal{B} + \frac{a}{h})(\alpha^2 + \beta^2) - 2\mathcal{A}\alpha\beta$ is positive if $a \geq e_1$.*

We set $Q = \alpha Q^+ + \beta Q^-$ with α, β two reals and Q^+, Q^- defined in (5), (8). Q satisfies:

$$\Delta Q = 0, \quad \text{in } \Upsilon, \quad Q = 0 \quad \text{on } \partial\hat{\Upsilon}, \quad \text{and} \quad \lim_{y_1 \rightarrow -\infty} \nabla Q = \beta \mathbf{e}_1, \quad \lim_{y_1 \rightarrow +\infty} \nabla Q = \alpha \mathbf{e}_1. \quad (37)$$

We define $H(y_1)$ with $H\left(y_1 < -\frac{e_1}{h}\right) = \beta\left(y_1 + \frac{e_1}{h}\right)$, $H\left(|y_1| \leq \frac{e_1}{h}\right) = 0$, $H\left(y_1 > \frac{e_1}{h}\right) = \alpha\left(y_1 - \frac{e_1}{h}\right)$, and $q = Q - H$ being continuous across any interfaces (in particular at $y_1 = \pm \frac{e_1}{h}$) and satisfying

$$q \underset{y_1 \rightarrow -\infty}{\sim} \alpha\mathcal{A} - \beta\left(\mathcal{B} + \frac{e_1}{h}\right), \quad q \underset{y_1 \rightarrow +\infty}{\sim} \alpha\left(\mathcal{B} + \frac{e_1}{h}\right) - \beta\mathcal{A}. \quad (38)$$

We define the restriction $\Upsilon^* \subset \Upsilon$ with $\Upsilon^* = \left\{ (y_1, y_2) \in (-y^*, y^*) \times (0, 1) \setminus \overline{\hat{\Upsilon}} \right\}$ and $y^* > e_1$. Integrating $q\Delta Q$ over Υ^* and using (37)-(38) gives

$$0 = \int_{\Upsilon^*} q\Delta Q \, d\mathbf{y} = - \int_{\Upsilon^*} \nabla q \cdot (\nabla q + \nabla H) \, d\mathbf{y} + (\alpha^2 + \beta^2) \left(\mathcal{B} + \frac{e_1}{h} \right) - 2\alpha\beta\mathcal{A} + o(y^*),$$

with $\lim_{y^* \rightarrow +\infty} o(y^*) = 0$. Next, integrating $H\Delta Q$ over Υ^* leads to

$$0 = \int_{\Upsilon^*} H\Delta Q \, d\mathbf{y} = - \int_{\Upsilon^*} \nabla H \cdot (\nabla q + \nabla H) \, d\mathbf{y} + (\alpha^2 + \beta^2) \left(y^* - \frac{e_1}{h} \right) + o(y^*).$$

Since $\int_{\Upsilon^*} \nabla H \cdot \nabla H \, d\mathbf{y} = (\alpha^2 + \beta^2) \left(y^* - \frac{e_1}{h} \right)$, and passing to the limit $y^* \rightarrow +\infty$, we finally find

$$0 \leq \int_{\Upsilon} \nabla q \cdot \nabla q \, d\mathbf{y} = \left(\mathcal{B} + \frac{e_1}{h} \right) (\alpha^2 + \beta^2) - 2\mathcal{A}\alpha\beta, \quad \forall (\alpha, \beta) \in \mathbb{R}^2.$$

We deduce that for $a \geq e_1$, $0 \leq (\mathcal{B} + \frac{a}{h})(\alpha^2 + \beta^2) - 2\mathcal{A}\alpha\beta$, $\forall(\alpha, \beta) \in \mathbb{R}^2$.

Transmission conditions have been implemented numerically using $a = e_1$, that is restoring the actual thickness of the array. The actual problem and the unified problem involving (35) have been implemented numerically in a consistent manner. In both cases, the numerical method combines a Finite Element scheme in space and a Finite Difference scheme in time [15]. P2 Finite Element are used on a triangular mesh along with a centered order 2 Newmark scheme in time, unconditionally stable without numerical damping [16].

5.2 Temporal evolution of the field in the cage

We consider now the 2D cage shown in figure 9; the linear array is composed of 10 circular wires of radius $e = 0.1$ (hence $e_1 = e$) and spacing $h = 1$ comprised in $x_2 \in (0, 10)$. The bottom boundary Γ^- at $x_1 = -5$ is associated with a Dirichlet boundary condition and radiation boundary conditions are imposed on Γ^+ at $x_1 = 10$. Eventually the lateral boundaries at $x_2 = 0$ and $x_2 = 10$ are associated with Neumann boundary condition.

Remark 5.2 *Note that in (12), Dirichlet condition was chosen on all boundaries for the ease of writing. This choice is however arbitrary and it does not affect the model whose essential ingredients are the transmission conditions; besides the analysis does not apply near the ends of the array where a specific analysis is required which is outside the scope of the present study (see [17]). In our simulations, Neumann boundary conditions on the lateral walls of the cavity avoids very small amplitudes within the cavity which would fall within numerical errors.*

We use a source S exciting a range of frequencies which includes the first 3 resonances of the cavity, namely $S(\mathbf{x}, t) = g(\mathbf{x})s(t)$, with $g(\mathbf{x}) = 1/\pi(0.1)^2$ within the disk centered at $(x_1 = 1, x_2 = 5)$ and of radius 0.1, $g(\mathbf{x}) = 0$ elsewhere. Next, $s(t) = e^{-\alpha t^2} \sin(\omega_s t)$ with $\alpha = 5 \cdot 10^{-3}$ and $\omega_s = 1$, see figure 8. For the actual problem on p , a refined mesh ($\Delta h = 10^{-2}$) is used in the vicinity of the wires to ensure that the near evanescent field of the order of e is well resolved; far from the wires, a coarser mesh ($\Delta h = 0.2$) ensures at least 16 points per wavelength up to $\omega \sim 2$. For the effective problem ruled by (35) with $a = e$, we have checked that a constant mesh step $\Delta h = 0.2$ is sufficient to produce converged solutions. In time, we use the same time step for both problems $\Delta t = 4 \cdot 10^{-2}$ to facilitate the comparison of the solutions.

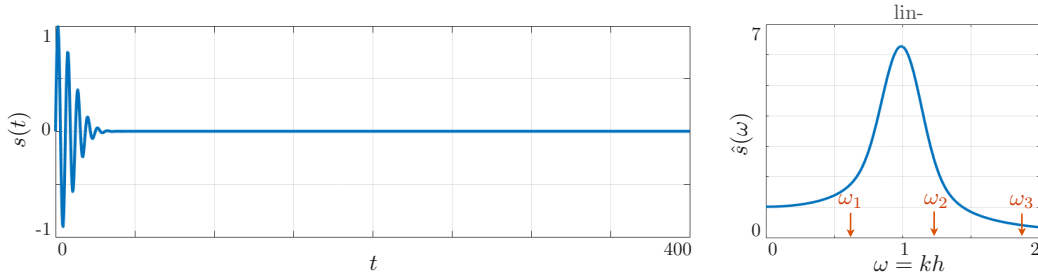


Figure 8: The source $s(t)$ and its Fourier transform $\hat{s}(\omega)$; the red arrows show the resonance frequencies of the cage.

To begin with, we report in figures 9 and 10 snapshots of the fields p and p^{ap} , both being computed numerically. Three regimes are exemplified:

- *The short times* – the source emits, part of the wave train hits the array and it is essentially reflected. The amplitude inside the cavity is weak as the shielding is efficient for most of the frequencies. However, we see in figure 9 that the field is not zero in the cavity both in the actual and effective problems. The cavity is little by little filled in.
- *The intermediate times* – the source is still emitting but with weaker amplitude. Meanwhile, the energy within the cavity has grown up. At these intermediate times, the amplitudes inside and outside the cavity are comparable.
- *The long times* – the source does not emit anymore and the waves issued from the source, directly or after reflection on the array, have left the calculation domain. Now the cavity releases energy very slowly, 'very slow' being related to the weak radiative damping of the cavity.

The agreement between both solutions is good at short times. More interestingly, the solutions keep on agreeing at intermediate and long times.

More quantitatively, we report in figure 11-left the time variations of the quantity $P(t)$ (resp. $P^{\text{ap}}(t)$) being the spatial average of $p(\mathbf{x}, t)$ (resp. $p^{\text{ap}}(\mathbf{x}, t)$) over the upper half-part of the cavity avoiding the near field of the wires in the actual geometry; we choose the domain $\Omega = \{(x_1, x_2) \in (0, 10) \times (-2.5, -2e)\}$, hence

$$P(t) = \int_{\Omega} p(\mathbf{x}, t) d\mathbf{x}, \quad P^{\text{ap}}(t) = \int_{\Omega} p^{\text{ap}}(\mathbf{x}, t) d\mathbf{x}. \quad (39)$$

The spectral content $\hat{P}(\omega)$ makes the first 3 resonance frequencies to appear. The quantitative agreement is excellent for $kh \in (0, 1)$, with a relative error less than 1%. It reaches 10% at the second resonance. Eventually, although

the trends around the third resonance are reasonably captured, the error reaches 100% very locally for $kh \in (1.77, 1.83)$ due to a small shift between the actual resonance and that predicted by the unified model.

5.3 Energetic aspects - stability of the model in time

In this section we move on to energetic aspects of the effective model and we address two different questions. Firstly, we have said that (35) ensure stability of the model for $a = e$ as used in the numerics reported in the previous section; we shall see that $a \geq a_c$ with $a_c \leq e$ is sufficient in a specific geometry that is when $(\mathcal{A}, \mathcal{B})$ are known. If $a < a_c$ numerical instabilities in time are fostered, resulting in a blow up of the solution $p^{\text{ap}}(\mathbf{x}, t)$. Next, the stability is associated with a positive interfacial energy \mathcal{E}_Γ whose link with the actual energy is inspected.

5.3.1 Stability of the model with enlarged transmission conditions

In the Lemma 5.1 we have established a criterion of stability of the enlarged transmission conditions (35); it is sufficient that $a \geq e$ to ensure the stability. The criterion can be refined for given $(\mathcal{A}, \mathcal{B})$; as \mathcal{E}_Γ in (36) is convex for $(\mathcal{B} + \frac{a}{h}) > 0$, $\mathcal{E}_\Gamma \geq 0$ if

$$a \geq a_c = h(|\mathcal{A}| - \mathcal{B}), \quad (40)$$

see ⁷. We report in figure 12-left the resulting stability diagram in the plane (a, e) for wires being discs or squares. In both cases, $(\mathcal{A}, \mathcal{B})$ are function of $e = e_1 = e_2$ only (the radius of the disc or the half-length of the square). It is visible that $a_c \sim e$ for squares while a_c is significantly lower than e for discs (in both cases, $a_c \leq e$). While the value of a is incidental in the harmonic regime, it is expected that $a < a_c$ produces numerical instability in the transient regime. We have used the transmission conditions (35) for various a around a_c ; for our wires with radius $e = 0.1$, the critical value of a is $a_c = 0.030$. A typical instability observed numerically by means of the blow-up in time of $p^{\text{ap}}(\mathbf{x}, t)$ is illustrated in figure 12-right; we have reported $|P^{\text{ap}}(t)|$ from (39) against t for a stable formulation $a > a_c$ (dashed black line, the solution is bounded) and for an unstable formulation $a < a_c$ (plain blue line, the solution blows up exponentially). In the inset for the unstable formulation, $\mathcal{E}_\Gamma(t; a) < 0$ diverges exponentially to $-\infty$ being roughly compensated by the exponential growth to $+\infty$ of the energy in the volume $\mathcal{E}^{\text{ap}}(t; a)$. "Roughly"

⁷ Denoting $\mathcal{B}_a = \mathcal{B} + \frac{a}{h} \geq 0$, $E(\alpha, \beta) = (\mathcal{B}_a(\alpha^2 + \beta^2) - 2\mathcal{A}\alpha\beta)$ can be positive if and only if $\mathcal{B}_a \geq 0$; in this case, $E(\alpha, \beta)$ is convex and its minimum with respect to α is $E_m(\beta) = \frac{1}{\mathcal{B}_a} (\mathcal{B}_a^2 - \mathcal{A}^2) \beta^2$. Hence $E \geq 0$ is guaranteed for $\mathcal{B}_a > |\mathcal{A}| > 0$.

means that the conservation of the energy (36) is not satisfied in our numerics when the fields have too large amplitudes. Note that the stability of the numerical solution in the close vicinity of $a = a_c$ depends on the mesh and time step; a complete analysis of this problem which is outside the scope of the present work requires to identify the discrete numerical energy associated with the numerical scheme.

5.3.2 Meaning of the interfacial energy \mathcal{E}_r

It is one thing to know that $a > a_c$ ensures the stability as it guaranties $\mathcal{E}_r(t; a) > 0$, it is quite another to interpret \mathcal{E}_r . Heuristically, \mathcal{E}_r approximates the sum of two actual energetic contributions : (i) that of the evanescent field being approximated by static fields (provided by the elementary problems) and (ii) that of the propagating field being approximated by linear fields (the loadings in the elementary problems). Up to now we have used $a = e$ hence $\mathcal{E}_r = \mathcal{E}_r(t; e)$ and we begin with this case. We have computed the actual and the effective energies

$$\begin{cases} \mathcal{E}_{\Omega_b}(t) = \frac{1}{2} \int_{\Omega_b} (\mathbf{u}^2 + p^2) \, d\mathbf{x} , & \Omega_b = \{(x_1, x_2) \in (-b, b) \times \Gamma\}, \\ \mathcal{E}_{\Omega_b}^{\text{ap}}(t) = \mathcal{E}_r(t; e) + \frac{1}{2} \int_{\Omega_b \setminus \Gamma_e} ((\mathbf{u}^{\text{ap}})^2 + (p^{\text{ap}})^2) \, d\mathbf{x} , & \Gamma_e = \{(x_1, x_2) \in (-e, e) \times \Gamma\}, \end{cases}$$

for $b \in (e, 5e)$. The results are reported in figure 13. The top panels show the fields $p(\mathbf{x}, t_0)$ and $p^{\text{ap}}(\mathbf{x}, t_0)$ in the vicinity of the wires ($t_0 = 19$); the contribution to p of the evanescent near-field is visible which is not reproduced by p^{ap} , by construction (the effect of the evanescent field has been encapsulated in the transmission conditions). As b increases, the domain Ω_b over which the energy is calculated increases. In the actual problem, \mathcal{E}_{Ω_b} increases accordingly being supplied by the evanescent field and by the propagating field. In contrast, in the effective problem, $\mathcal{E}_{\Omega_b}^{\text{ap}}$ increases being supplied by the propagating field only, as \mathcal{E}_r approximates the whole energy of the evanescent field. We expect the two energies to coincide (up to the error of the model) when b is large enough so that the actual energy also contains the whole energy of the evanescent field. The results in figure 13 support this scenario. We observe that $\mathcal{E}_{\Omega_b}^{\text{ap}} > \mathcal{E}_{\Omega_b}$ up to $b \simeq 2.5e$ afterwards the two energies coincide up to a relative error (about 5%) attributable to the error of the model.

We now move to the influence of a , the enlargement of the interface. We have computed $\mathcal{E}_r(t; a)$ for $a \in (0.10, 0.25)$ that we compare to its counterpart in the actual problem

$$\mathcal{E}_{\Omega_a}(t) = \frac{1}{2} \int_{\Omega_a} (\mathbf{u}^2 + p^2) \, d\mathbf{x} , \quad \Omega_a = \{(x_1, x_2) \in (-a, a) \times \Gamma\}.$$

From what we have seen from the previous representation, we could expect that $\mathcal{E}_r(t; a) \simeq \mathcal{E}_{\Omega_a}(t)$ as soon as $a > 2.5e$ that is as soon as \mathcal{E}_{Ω_a} contains the whole contribution of the evanescent field. This is not the case as illustrated in figures 14 and 15; the reason relies this time on the contribution of the propagating field. For every a , $\mathcal{E}_r(t; a)$ approximates the energetic contribution of the evanescent field but it has also to approximate that of the propagating field. The propagating field is approximated by its expansions, a constant at zero order and a linear function at the first order; hence, the approximation becomes cruder as a increases. It results that the ability of $\mathcal{E}_r(t; a)$ to resemble \mathcal{E}_{Ω_a} is a compromise between the actual extension of the evanescent field and the validity of a linear approximation of the propagating field. From figure 14, it is visible that for small a $\mathcal{E}_r(t; a) > \mathcal{E}_{\Omega_a}$ as the contribution of the evanescent field is incomplete in \mathcal{E}_{Ω_a} ; reversely, for large a , $\mathcal{E}_r(t; a) < \mathcal{E}_{\Omega_a}$ indicating that $\mathcal{E}_r(t; a)$ underestimates the contribution of the propagating field. The compromise is obtained for $a \sim 1.6e$, although it is visible from figure 15 that the evanescent field is still strong at $x_1 = 1.6e$.

Note that, if the comparison of $\mathcal{E}_r(t; a)$ and $\mathcal{E}_{\Omega_a}(t)$ is enlightening on the meaning of the interfacial energy, there is no guaranty that the value of a minimizing their difference coincide with the value of a minimizing the error between p and p^{sp} in the far field. (In the temporal regime, we do not find a clear minimum of this error as a varies; in the harmonic regime, we have observed a minimum in the scattering coefficients for $a \simeq 1.5e$ ⁸.)

6 Concluding remarks and perspectives

We have shown both theoretically and numerically that the transmission conditions derived in [10, 11] for an array of Dirichlet wires in free space apply without additional work when the array delimits a resonant cavity. These conditions, called unified conditions in the present study, have several advantages, (i) they are valid at any frequency and for any size of the wires, (ii) in their enlarged version, they guaranty stability in the transient regime. The point (i) is linked to the fact that the unified conditions avoid an iterative resolution of the asymptotic problems which is at the origin of the problem stressed in [7]. (The zero order problem is ill-posed at the resonance frequen-

⁸ The question of the value of a producing the best approximation of the actual solution does not have a theoretical answer. Besides, the answer is not universal; in [12] for a 3-phase array distributed on a circle, increasing the values of a produces larger errors, in [18] for a 2-phase linear array a minimum of the error was found to occur for $a = e$, in [19] for a rough Neumann boundary the optimal value was shown to vary with the geometry of the roughness.

cies of the closed cavity.) The point (ii) is linked to the fact that the effective problem in its enlarged version is associated with a positive interfacial energy which prevents from numerical instabilities.

More generally, we can remark that the construction of a unified, or unique, problem gathering the results of the asymptotic analysis up to first order (or higher orders) follows the construction of the models of continuum mechanics or continuum physics. As for these classical models, the properties of new homogenized models can be analyzed in all generality, independently of the specific context in which they will be used, as the sources and the surrounding boundaries. In contrast, an iterative resolution focuses on a specific solution for given sources and surrounding boundaries. As such it reduces the range of applicability of the homogenization, as the work has to be done for each new problem. Besides, as in the exemple reported in this study, it can lead to unnecessary complications.

Eventually, in a dynamical context of wave propagation, we stress the interest of establishing the effective models in the time domain in order to check the good energetic properties, conservation of a positive energy in the bulk and of the fluxes of energy. (We have given an illustration of the blow-up of the numerical solution in time when these properties are not satisfied.)

We have no competing interests.

The numerical results of the direct problem in the harmonic regime were obtained using a standard multimodal method as presented in Marigo J.-J., Maurel A. 2017 *An interface model for homogenization of acoustic metafilms*. World Scientific Handbook of Metamaterials and Plasmonics Volume 2: Elastic, Acoustic, and Seismic Metamaterials. The numerical results in the transient regime were obtained using the FEM-BEM C++ code XLiFE++, see also [15].

B.D, J-F. M and E.L. realised the numerics in the transient regime. A.M. and K.P. realised the numerics in the harmonic regime. All authors participated in the modelling and analysis, contributed to the paper, gave final approval for publication and agree to be held accountable for the work performed therein.

Kim Pham thanks the support of the Agence de l’Innovation de Défense (AID) from the Direction Générale de l’Armement (DGA), under grant 2019 65 0070.

We thank the peer reviewers for their constructive comments.

A Step by step derivation of the resonant cases

In this Appendix, we use the Ansatz (16). We shall use the following result: any harmonic function $q(\mathbf{y})$ in \mathbf{Y} satisfying a homogeneous Dirichlet condition

on $\partial\hat{Y}$ and with no exponential growth when y_1 goes to $\pm\infty$ can be written as

$$q(\mathbf{y}) = aQ^-(\mathbf{y}) + bQ^+(\mathbf{y}), \quad (41)$$

where Q^\pm are defined in (5) and (6).

Remark A.1 *For the sake of concision, the proof of existence and uniqueness of Q^- and Q^+ is not written here (see e.g [8]) . It is based on the application of the Lax-Milgram Lemma together with a Hardy-equality [20, Lemma 2.5.7]. A crucial point is that there is no harmonic function in Y satisfying a homogeneous Dirichlet condition on $\partial\hat{Y}$ and behaving like a constant as y_1 goes to both $\pm\infty$.*

A.1 The near-resonant case (2i): $\kappa_1 \neq \kappa$

In that case, we make the Ansatz (16) with $m_0 = 0$. Inserting the formal series into Equation (12) and separating the different powers of ε leads to a collection of equations for the near and far field terms. These equations are linked with the matching conditions that enforces the far and near field expansions to coincide in some intermediate area (see e.g.[12, 21, 10]). In the present case, they can be written as

$$p_i(0^\pm, x_2) = \lim_{y_1 \rightarrow \pm\infty} \left(\sum_{m=1}^{i-m_0} \frac{(y_1)^m}{m!} \frac{\partial^m p_{i-m}}{\partial x_1^m}(0^\pm, x_2) - q_i(\mathbf{y}, x_2) \right) \quad i \geq -1. \quad (42)$$

By convention, the previous sum is empty (and vanishes) if $i - m_0 < 1$. First, the leading order far field term p_0 and near field term q_0 (1-periodic *w.r.t* y_2) are solutions to:

$$\begin{cases} \Delta p_0 + K_n^* p_0 = S & \text{in } \Omega^\pm, \\ \frac{\partial p_0}{\partial x_1} = i\sqrt{K_n^*} p_0 & \text{on } \Gamma^+, p_0 = 0 & \text{on } (\partial\Omega^- \cup \partial\Omega^+) \setminus (\Gamma^+ \cup \Gamma), \end{cases} \quad \begin{cases} \Delta q_0 = 0 & \text{in } Y, \\ q_0 = 0 & \text{on } \partial\hat{Y}, \end{cases} \quad (43)$$

complemented (and linked) by the zero order matching conditions (42) ($i = 0$). In (43-right) Y denotes the periodicity cell $Y = \left\{ (y_1, y_2) \in \mathbb{R} \times \left(-\frac{1}{2}, \frac{1}{2}\right) \setminus \bar{Y} \right\}$.

Using (41), q_0 can be written as $q_0(\mathbf{y}, x_2) = a(x_2)Q^-(\mathbf{y}) + b(x_2)Q^+(\mathbf{y})$, and the matching condition indicates that q_0 tends to constants as y_1 goes to $\pm\infty$. From Remark A.1, we get $a(x_2) = b(x_2) = 0$, hence $p_0(0^\pm, x_2) = 0$. These conditions complement the Problem (43-left), and the solution reads

$$p_0 = P_n^* \quad \text{in } \Omega^+ \quad \text{and} \quad p_0 = \alpha_1 p_n^* \quad \text{in } \Omega^-, \quad (44)$$

where P_n^* is the unique solution to (13-left) and p_n^* is defined in (19). It remains to determine α_1 . In fact, the value of α_1 is imposed by the solvability condition associated with the far field problem of order 1 in Ω^- . More specifically, we have

$$\begin{cases} \Delta p_1 + K_n^* p_1 = -\kappa_1 \alpha_1 p_n^* & \text{in } \Omega^-, \\ p_1 = 0 & \text{on } \partial\Omega^- \setminus \Gamma, \end{cases} \quad \begin{cases} \Delta q_1 = 0 & \text{in } \Upsilon, \\ q_1 = 0 & \text{on } \partial\hat{\Upsilon}, \end{cases} \quad (45)$$

with q_1 1-periodic *w.r.t.* y_2 and the first order matching conditions (42) ($i = 1$). As previously, we look for $q_1(\mathbf{y}, x_2) = a(x_2)Q^-(\mathbf{y}) + b(x_2)Q^+(\mathbf{y})$. Identifying in the matching conditions the parts linear in y_1 and the constants, we get $a(x_2) = \frac{\partial p_0}{\partial x_1}(0^-, x_2)$, $b(x_2) = \frac{\partial p_0}{\partial x_1}(0^+, x_2)$, hence $p_1(0^-, x_2) = -\mathcal{B}a(x_2) + \mathcal{A}b(x_2)$, $p_1(0^+, x_2) = -\mathcal{A}a(x_2) + \mathcal{B}b(x_2)$, and using (44)

$$\begin{cases} q_1(\mathbf{y}, x_2) = \alpha_1 \frac{\partial p_n^*}{\partial x_1}(0, x_2) Q^-(\mathbf{y}) + \frac{\partial P_n^*}{\partial x_1}(0, x_2) Q^+(\mathbf{y}), \\ p_1(0^-, x_2) = \mathcal{A} \frac{\partial P_n^*}{\partial x_1}(0, x_2) - \alpha_1 \mathcal{B} \frac{\partial p_n^*}{\partial x_1}(0, x_2). \end{cases}$$

Finally, integrating over Ω^- (45-left) after multiplication by p_n^* and integrating by part, we see that Problem (45-left) is solvable if and only if

$$\alpha_1 \left(\kappa_1 + \mathcal{B} \int_{\Gamma} \left(\frac{\partial p_n^*}{\partial x_1}(0, x_2) \right)^2 dx_2 \right) = \mathcal{A} \int_{\Gamma} \frac{\partial P_n^*}{\partial x_1}(0, x_2) \frac{\partial p_n^*}{\partial x_1}(0, x_2) dx_2.$$

In view of the definition (20) of κ and since by assumption $\kappa_1 \neq \kappa$, the previous equation entirely defines α_1 in (44).

A.2 The on-resonance case (2ii) : $\kappa_1 = \kappa$

In that case, we still make the Ansatz (16) but we found $m_0 = -1$ (reflecting the presence of a strong resonant effect).

A.2.1 The leading order: $i = -1$

As previously, the far field term p_{-1} and near field term q_{-1} (1-periodic *w.r.t.* y_2) are solutions to:

$$\begin{cases} \Delta p_{-1} + K_n^* p_{-1} = 0 & \text{in } \Omega^\pm, \\ \frac{\partial p_{-1}}{\partial x_1} = i\sqrt{K_n^*} p_{-1} \text{ on } \Gamma^+, p_{-1} = 0 \text{ on } (\partial\Omega^- \cup \partial\Omega^+) \setminus (\Gamma^+ \cup \Gamma), \end{cases} \quad \begin{cases} \Delta q_{-1} = 0 & \text{in } \Upsilon, \\ q_{-1} = 0 & \text{on } \partial\hat{\Upsilon}, \end{cases} \quad (46)$$

complemented by the matching conditions (42) for $i = -1$. As previously, we deduce from the near field equation (46-right) that $q_{-1}(\mathbf{y}, x_2) = a(x_2)Q^-(\mathbf{y}) + b(x_2)Q^+(\mathbf{y})$, hence again, as (42) imposes that q_{-1} tends to a constant as y_1 goes to $\pm\infty$, we obtain that $a(x_2) = b(x_2) = 0$, and therefore $q_{-1} = 0$. Consequently $p_{-1}(0^\pm, x_2) = 0$. Together with (46-left), we deduce that

$$p_{-1} = 0 \quad \text{in } \Omega^+, \quad \text{and} \quad p_{-1} = \alpha_2 p_n^* \quad \text{in } \Omega^-, \quad (47)$$

where p_n^* is defined in (19), the constant α_2 being undetermined at this stage. Expectedly, in the absence of a source term at the order $i = -1$, the field outside the cavity is zero at this order.

A.2.2 The order $i = 0$

The analysis of the leading order provides neither the leading order asymptotic for p^ε in Ω^+ nor the constant α_2 . Therefore, we need to analyse p_0 and q_0 (1-periodic *w.r.t.* y_2) solutions to:

$$\begin{cases} \Delta p_0 + K_n^* p_0 = S & \text{in } \Omega^+, \\ \frac{\partial p_0}{\partial x_1} = i\sqrt{K_n^*} p_0 & \text{on } \Gamma^+, \quad p_0 = 0 & \text{on } \partial\Omega^+ \setminus (\Gamma^+ \cup \Gamma), \end{cases} \quad \begin{cases} \Delta p_0 + K_n^* p_0 = -\kappa\alpha_2 p_n^* & \text{in } \Omega^-, \\ p_0 = 0 & \text{on } \partial\Omega^- \setminus \Gamma, \end{cases} \quad (48)$$

$$\Delta q_0 = 0 \quad \text{in } \Upsilon, \quad q_0 = 0 \quad \text{on } \partial\hat{\Upsilon}, \quad (49)$$

together with the zero order matching conditions (42) and using (47). Looking for $q_0(\mathbf{y}, x_2) = a(x_2)Q^-(\mathbf{y}) + b(x_2)Q^+(\mathbf{y})$ and identifying in the matching conditions the parts linear in y_1 and the constants, we get $a(x_2) = \alpha_2 \frac{\partial p_n^*}{\partial x_1}(0, x_2)$ and $b(x_2) = 0$, hence

$$q_0(\mathbf{y}, x_2) = \alpha_2 \frac{\partial p_n^*}{\partial x_1}(0, x_2) Q^-(\mathbf{y}), \quad p_0(0^+, x_2) = -\mathcal{A} \alpha_2 \frac{\partial p_n^*}{\partial x_1}(0, x_2), \quad p_0(0^-, x_2) = -\mathcal{B} \alpha_2 \frac{\partial p_n^*}{\partial x_1}(0, x_2). \quad (50)$$

The above relations provide $p^0(0^\pm, x_2)$ which complement the Problems (48) set in Ω^+ and Ω^- ; at this stage, they are disconnected. In Ω^+ , p_0 solution to (48-left) along with (50-center) reads

$$p_0(\mathbf{x}) = \alpha_2 \mathcal{A} P^+(\mathbf{x}) + P_n^*(\mathbf{x}) \quad \text{in } \Omega^+, \quad (51)$$

where P^+ and P_n^* are the (unique) solutions to (25-left) and (13-left). It then provides the asymptotic behavior of p^ε in Ω^+ (up to the definition of α_2). In Ω^- , since K_n^* is a resonance frequency, the far field problem (48-right)-(50-right) is not well-posed (it has a kernel of dimension 1 spanned by p_n^*):

However, it is solvable. Indeed, multiplying (48-right) by p_n^* and integrating over Ω^- gives

$$\alpha_2 \left(\kappa + \mathcal{B} \int_{\Gamma} \left(\frac{\partial p_n^*}{\partial x_1}(0, x_2) \right)^2 dx_2 \right) = 0,$$

and the above equality is fulfilled for any α_2 by definition of κ (see (20)). It follows that p_0 solution to (48-right) along (50-right) reads

$$p_0(\mathbf{x}) = \alpha_2 \mathcal{B} P^-(\mathbf{x}) + \beta p_n^*(\mathbf{x}) \quad \text{in } \Omega^-, \quad (52)$$

where P^- is the unique solution to (25-right) and p_n^* is the real-valued eigenvector associated with K_n^* (for the cavity problem (13-right)). In (52), α_2 that reaches back from the order $i = -1$ (see (47)) and β are constants that remain to be determined.

A.2.3 The order $i = 1$

Here, we shall determine the constant α_2 that we need to parametrize locally the resonance curve. To do so, it is enough to investigate the solvability of the far field problem for p_1 in Ω^- and the near field problem for q_1 (1-periodic w.r.t. y_2), namely,

$$\begin{cases} \Delta p_1 + K_n^* p_1 = -\kappa p_0 - \kappa_2 \alpha_2 p_n^* & \text{in } \Omega^-, \\ p_0 = \alpha_2 \mathcal{B} P^- + \beta p_n^*, p_1 = 0, & \text{on } \partial\Omega^- \setminus \Gamma, \end{cases} \quad \begin{cases} \Delta q_1 = -2\alpha_2 \frac{\partial^2 p_n^*}{\partial x_1 \partial x_2}(0, x_2) \frac{\partial Q^-}{\partial y_2} & \text{in } \Upsilon, \\ q_1 = 0 & \text{on } \partial\hat{\Upsilon}. \end{cases} \quad (53)$$

We have used the forms of p_{-1} in (47), of p_0 in (52) and of q_0 in (50). The two problems are complemented by the matching conditions (42) at order -1 ($i = -1$) with $\frac{\partial^2 p_{-1}}{\partial x_1^2}(0^\pm, x_2) = 0$. We define Q , 1-periodic w.r.t. y_2 , unique solution to

$$\Delta Q = -2 \frac{\partial Q^-}{\partial y_2} \quad \text{in } \Upsilon, \quad Q = 0 \quad \text{on } \partial\hat{\Upsilon}, \quad \lim_{y_1 \rightarrow \pm\infty} \nabla Q = \mathbf{0}. \quad (54)$$

(Here again, see Remark A.1, the well-posedness of (54) results from the Lax-Milgram Lemma.) As $\tilde{q}_1 = (q_1 - \alpha_2 \frac{\partial^2 p_n^*}{\partial x_1 \partial x_2}(0, x_2) Q)$ satisfies $\Delta \tilde{q}_1 = 0$ with $\tilde{q}_1 = 0$ on $\partial\hat{\Upsilon}$, we look for q_1 of the form

$$q_1(\mathbf{y}, x_2) = a(x_2) Q^-(\mathbf{y}) + b(x_2) Q^+(\mathbf{y}) + \alpha_2 \frac{\partial^2 p_n^*}{\partial x_1 \partial x_2}(0, x_2) Q(\mathbf{y}).$$

Inserting q_1 in (53-right), identifying the parts linear in y_1 and the constants, we obtain that

$$q_1(\mathbf{y}, x_2) = \frac{\partial p_0}{\partial x_1}(0^-, x_2)Q^-(\mathbf{y}) + \frac{\partial p_0}{\partial x_1}(0^+, x_2)Q^+(\mathbf{y}) + \alpha_2 \frac{\partial^2 p_n^*}{\partial x_1 \partial x_2}(0, x_2)Q(\mathbf{y}),$$

$$p_1(0^-, x_2) = -\mathcal{B} \frac{\partial p_0}{\partial x_1}(0^-, x_2) + \mathcal{A} \frac{\partial p_0}{\partial x_1}(0^+, x_2).$$

Eventually, using p_0 given by (51) and (52), we end up with

$$p_1(0^-, x_2) = \alpha_2 \left((\mathcal{A})^2 \frac{\partial P^+}{\partial x_1} - (\mathcal{B})^2 \frac{\partial P^-}{\partial x_1} \right)_{|x_1=0} + \left(\mathcal{A} \frac{\partial P_n^*}{\partial x_1} - \mathcal{B} \beta \frac{\partial p_n^*}{\partial x_1} \right)_{|x_1=0},$$

which complements Problem (53-left). It is now sufficient to multiply (53-left) by p_n^* and to integrate over Ω^- to see that Problem (53-left) is solvable if and only if $\alpha_2 \kappa_2 = \int_{\Gamma} p_1 \frac{\partial p_n^*}{\partial x_1}(0, x_2) dx_2 - \kappa \int_{\Omega^-} p_0 p_n^* d\mathbf{x}$, resulting in

$$\alpha_2 \left[\kappa_2 - (\mathcal{A})^2 \int_{\Gamma} \left(\frac{\partial P^+}{\partial x_1} \frac{\partial p_n^*}{\partial x_1} \right)_{|x_1=0} dx_2 + (\mathcal{B})^2 \int_{\Gamma} \left(\frac{\partial P^-}{\partial x_1} \frac{\partial p_n^*}{\partial x_1} \right)_{|x_1=0} dx_2 \right] = \mathcal{A} \int_{\Gamma} \left(\frac{\partial P_n^*}{\partial x_1} \frac{\partial p_n^*}{\partial x_1} \right)_{|x_1=0} dx_2, \quad (55)$$

as mentioned in (23) (with (22) and (24)). In (55), note that the term in β has canceled; also, we have used that P^- is orthogonal to p_n^* . Also, we have used that $\lim_{y_1 \rightarrow \pm\infty} Q = 0$ for wires symmetric *w.r.t* y_2 , as Q is an odd function of y_2 ; the result (55) on α_2 holds for any wire shape.

B The Elementary problem

Here, we report additional informations on the effective parameters $(\mathcal{A}, \mathcal{B})$ issued from the elementary solution Q^+ to (5): Figure 16-right shows an example of the fields $Q^+(\mathbf{y})$ for a wire being a disk or a square, and Figure 16-left show the variations of $(\mathcal{A}, \mathcal{B})$ against $\frac{e}{h}$; values of $(\mathcal{A}, \mathcal{B})$ used for squares (in the harmonic regime) and for disks (in the transient regime) throughout the paper are given in the table (56).

e (half square length)	\mathcal{A}	\mathcal{B}	e (disk radius)	\mathcal{A}	\mathcal{B}
0.01	0.4143	0.4138	0.01	0.4411	0.4407
0.1	0.0684	0.0265	0.1	0.0892	0.0588
0.2	0.0088	-0.1384	0.2	0.0178	-0.0932

(56)

C The thin wire approximation

The thin wire approximation presented in [7] allows to capture the leakage of the cavity at the dominant order. The reason is that the amplitude within the cavity is of order ε including at the resonance frequency. (This is already visible in figure 5 for $e = 0.01h$ where the amplitude \mathcal{P}_{\max} does not overcome 0.1.) This is obtained by choosing a scaling $\frac{e}{h} = O(e^{-\frac{c}{\varepsilon}})$ (with c a constant), which means that the wire thickness e vanishes exponentially faster than the array spacing h when ε goes to zero. In this case it is found that

$$p^{\text{tw}}(0, \mathbf{x}_2) = h\mathcal{A}_0 \left(\frac{\partial p^{\text{tw}}}{\partial x_1}(0^+, \mathbf{x}_2) - \frac{\partial p^{\text{tw}}}{\partial x_1}(0^-, \mathbf{x}_2) \right), \quad (57)$$

with p^{tw} continuous. Expectedly, the above condition is consistent with the formulation (7) when $\mathcal{A} = \mathcal{B} = \mathcal{A}_0$. For the simple scattering problem considered in §4, the solution reads as in (29) with

$$\mathcal{R}^{\text{ap}} = -\frac{\bar{z}}{z}, \quad \mathcal{P}^{\text{ap}} = -\frac{2ikc_\theta h\mathcal{A}_0}{z}, \quad z = 1 + kc_\theta h\mathcal{A}_0(\cos(kc_\theta D) - i\sin(kc_\theta D)), \quad (58)$$

and $\mathcal{A}_0 = -\frac{1}{2\pi} \log(\sin \frac{2\pi e}{h})$, which is consistent with (29)-(30) in the considered limit. We report the resonance curves in figure 17 as in figure 5. The thin wire model appears to more limited, its accuracy depending on how close $(\mathcal{A}, \mathcal{B})$ are to their asymptotic value \mathcal{A}_0 .

References

- [1] Chen CC. 1971 Diffraction of electromagnetic waves by a conducting screen perforated periodically with holes. *IEEE Transactions on Microwave Theory and Techniques* **19**, 475–481.
- [2] McPhedran R, Maystre D. 1977 On the theory and solar application of inductive grids. *Applied physics* **14**, 1–20.
- [3] McPhedran R, Derrick G, Botten L. 1980 Theory of crossed gratings. In: Petit R. (eds) *Electromagnetic Theory of Gratings* pp. 227–276. Springer.
- [4] Ulrich R. 1968 Interference filters for the far infrared. *Applied Optics* **7**, 1987–1996.
- [5] Martin P. 2014 On acoustic and electric Faraday cages. *Proc. R. Soc. A* **470**, 20140344.

- [6] Chapman SJ, Hewett DP, Trefethen LN. 2015 Mathematics of the Faraday cage. *Siam Review* **57**, 398–417.
- [7] Hewett DP, Hewitt IJ. 2016 Homogenized boundary conditions and resonance effects in Faraday cages. *Proc. R. Soc. A* **472**, 20160062.
- [8] Delourme B, Hewett DP. 2020 Electromagnetic shielding by thin periodic structures and the Faraday cage effect. *Comptes Rendus. Mathématique* **358**, 777–784.
- [9] Felbacq D, Bouchitté G. 1997 Homogenization of a set of parallel fibres. *Waves in random media* **7**, 245–256.
- [10] Marigo JJ, Maurel A. 2016 Two-scale homogenization to determine effective parameters of thin metallic-structured films. *Proc. R. Soc. A* **472**, 20160068.
- [11] Maurel A, Marigo JJ, Ourir A. 2016 Homogenization of ultrathin metallo-dielectric structures leading to transmission conditions at an equivalent interface. *JOSA B* **33**, 947–956.
- [12] Delourme B . 2010 Modèles et asymptotiques des interfaces fines et périodiques en électromagnétisme. *PhD thesis, U. Pierre et Marie Curie, France*.
- [13] Delourme B, Haddar H, Joly P. 2012 Approximate models for wave propagation across thin periodic interfaces. *Journal de mathématiques pures et appliquées* **98**, 28–71.
- [14] David M, Marigo JJ, Pideri C. 2012 Homogenized interface model describing inhomogeneities located on a surface. *Journal of Elasticity* **109**, 153–187.
- [15] <https://uma.ensta-paris.fr/soft/XLiFE++/>
- [16] Bathe KJ, Wilson EL. 1976 *Numerical methods in finite element analysis*. Number BOOK. Prentice-Hall.
- [17] Semin A, Delourme B, Schmidt K. 2018 On the homogenization of the Helmholtz problem with thin perforated walls of finite length. *ESAIM: Mathematical Modelling and Numerical Analysis* **52**, 29–67.
- [18] Marigo JJ, Maurel A, Pham K, Sbitti A. 2017 Effective dynamic properties of a row of elastic inclusions: The case of scalar shear waves. *Journal of elasticity* **128**, 265–289.

- [19] Maurel A, Marigo JJ, Pham K. 2018 Effective boundary condition for the reflection of shear waves at the periodic rough boundary of an elastic body. *Vietnam J. Mech* **40**, 303–323.
- [20] Nédélec JC. 2001 *Acoustic and electromagnetic equations: integral representations for harmonic problems*. Springer Science & Business Media.
- [21] Maz'Ya V, Nazarov S, Plamenevskij B. 2012 *Asymptotic theory of elliptic boundary value problems in singularly perturbed domains* vol. 1. Birkhäuser.

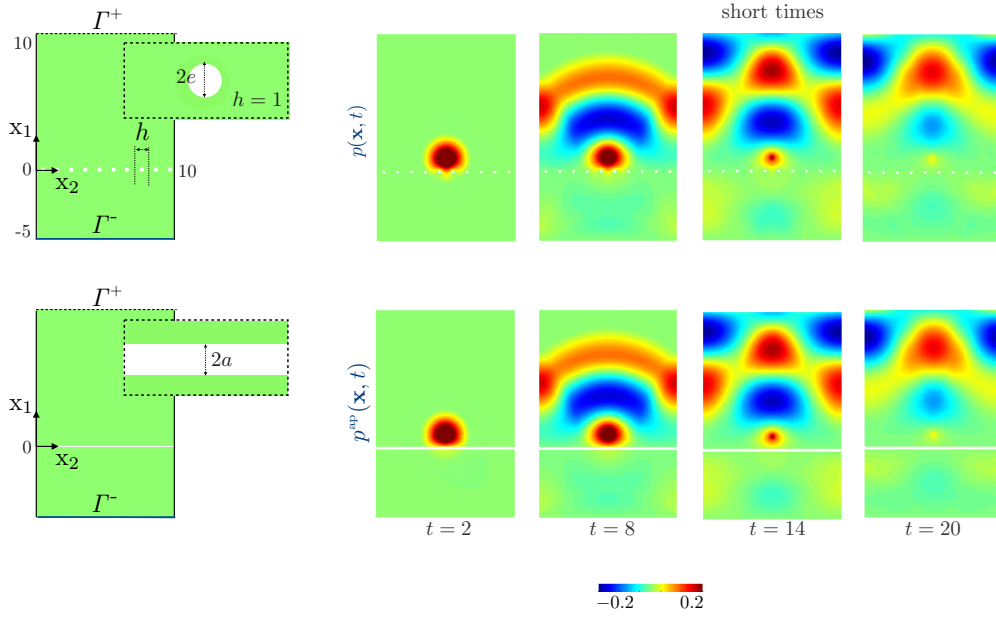


Figure 9: Snapshots at short times – $p(\mathbf{x}, t)$ solution of the actual problem (top panels) and of $p^{\text{ap}}(\mathbf{x}, t)$ solution of the effective problem ruled by (35) with $a = e$ (bottom panels); both p and p^{ap} are computed numerically.

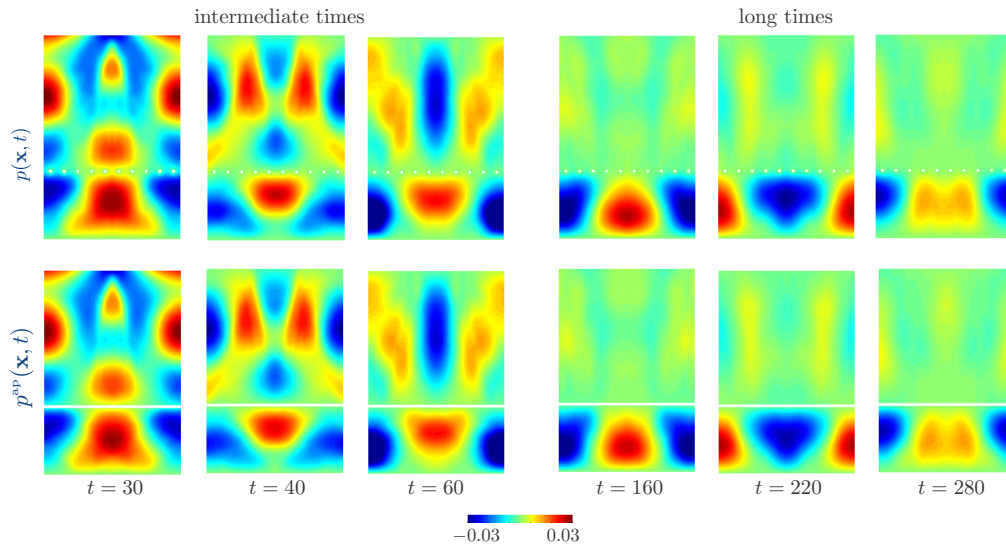


Figure 10: Same representation as in figure 9 at intermediate times and at long times.

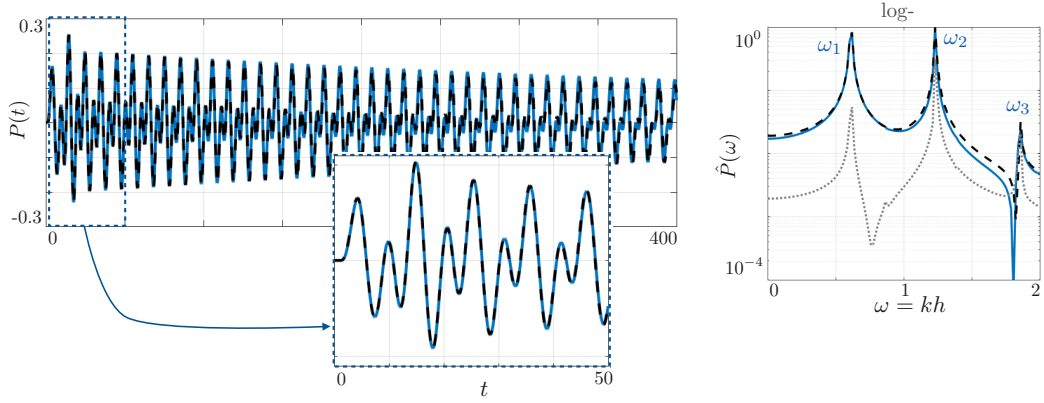


Figure 11: Left: Time variation of $P(t)$ (plain blue line) and of $P^{\text{ap}}(t)$ (dashed black line) for $t \in (0, 400)$. Right: corresponding spectra $\hat{P}(\omega)$ and $\hat{P}^{\text{ap}}(\omega)$; the dotted grey line shows the spectrum of the error $|p^{\text{ap}} - p|$.

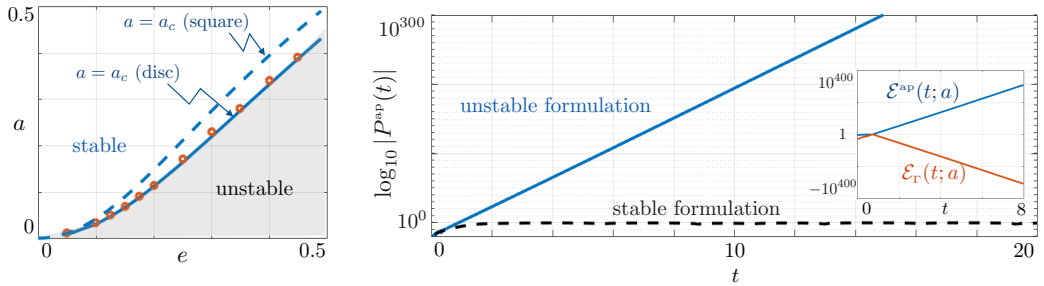


Figure 12: Numerical instability in the effective problem ruled by unstable conditions (35) when $a < a_c$ – Left: Stability diagram for discs and squares. Blue lines show $a_c(e)$ from (40) for wires of extend e . The red symbols show an estimate of a_c determined numerically as the lowest value of a producing a stable solution. Right: exponential growth in time of $|P^{\text{ap}}(t)|$, (39), for an unstable formulation ($a = 0.015 < a_c$, plain blue lines) and for a stable formulation ($a = 0.033 > a_c$, dashed black lines). The inset shows $\mathcal{E}^{\text{ap}}(t; a)$ diverging to $+\infty$ and $\mathcal{E}_r(t; a)$ diverging to $-\infty$ for $a = 0.015$.

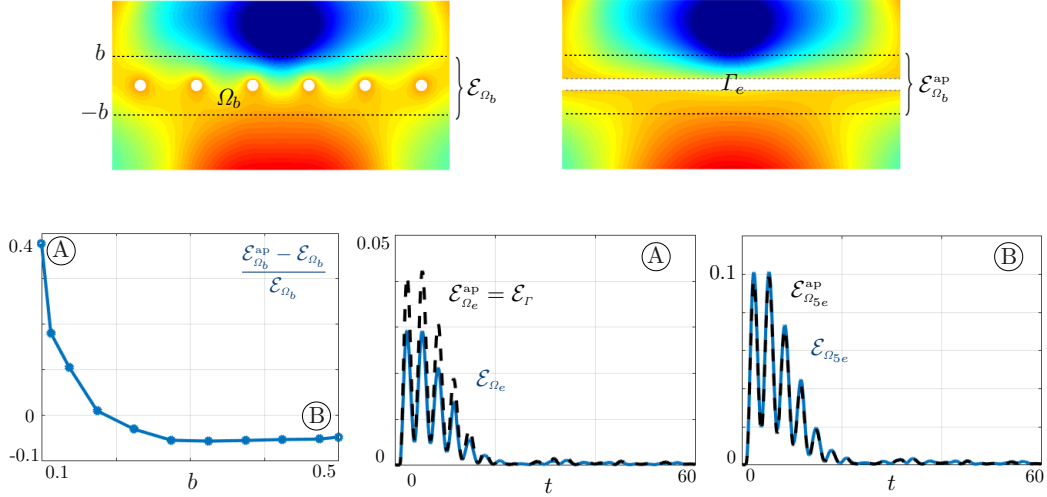


Figure 13: Energies in the actual and effective problems – Top panels show a zoom of $p(\mathbf{x}, t_0)$ and $p^{\text{ap}}(\mathbf{x}, t_0)$ in $\{(x_1, x_2) \in (-1.5, 1.5) \times (-3, 3)\}$ ($t_0 = 19$). Bottom panels show the difference between the time averaged energies $\mathcal{E}_{\Omega_b}^{\text{ap}}$ and \mathcal{E}_{Ω_b} against b and time variations of the energies for \textcircled{A} $b = e = 0.1$ and \textcircled{B} $b = 5e = 0.5$.

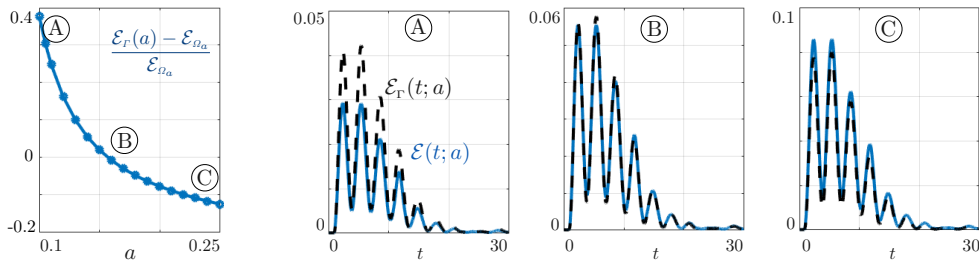


Figure 14: Relative difference between the time averaged interface effective energy $\mathcal{E}_\Gamma(a)$ and the time averaged actual energy \mathcal{E}_{Ω_a} against a ; time variations of $\mathcal{E}_\Gamma(t; a)$ (dashed black lines) and $\mathcal{E}(t; a)$ (blue plain lines) for \textcircled{A} $a = 0.1$, \textcircled{B} $a = 0.15$ and \textcircled{C} $a = 0.25$.

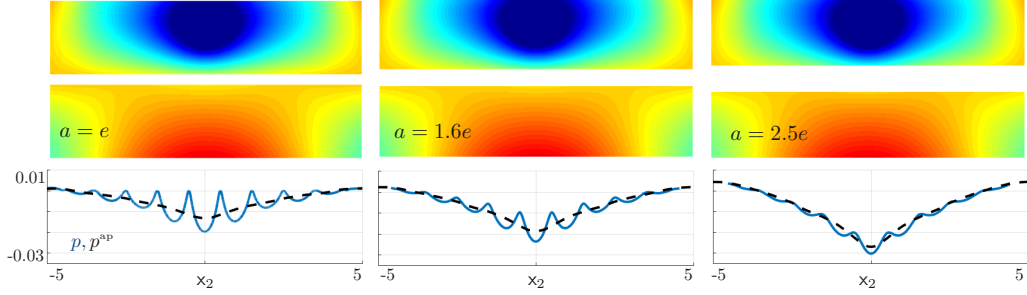


Figure 15: Effective fields $p^{\text{ap}}(\mathbf{x}, t_0)$ ($t_0 = 19$) in the vicinity of Γ for $a = 0.1$, $a = 0.16$ and $a = 0.25$ (top panels) and corresponding profiles of p (blue plain lines) and p^{ap} (dashed black lines) at $x_1 = a$ (bottom panels).

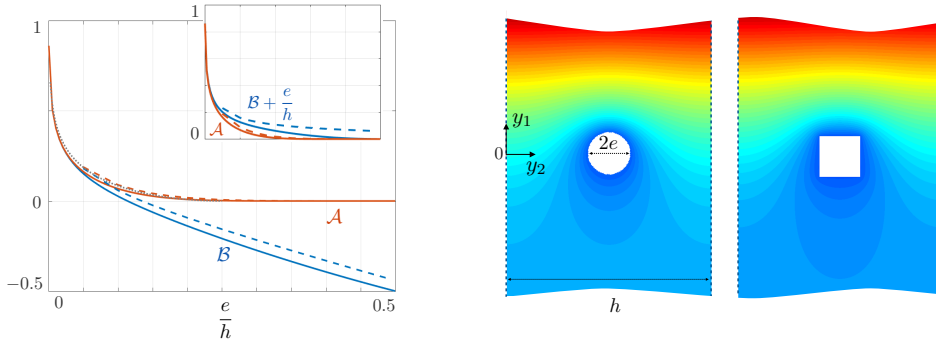


Figure 16: Left: effective parameters (\mathcal{A}, \mathcal{B}) against $\frac{e}{h}$ for squares (plain lines) and for disks (dashed lines); the dotted grey line shows $\mathcal{A}_0 = -\frac{1}{2\pi} \log \sin\left(\frac{2\pi e}{h}\right)$. Right: Examples of solution Q^+ to the elementary problem (5).

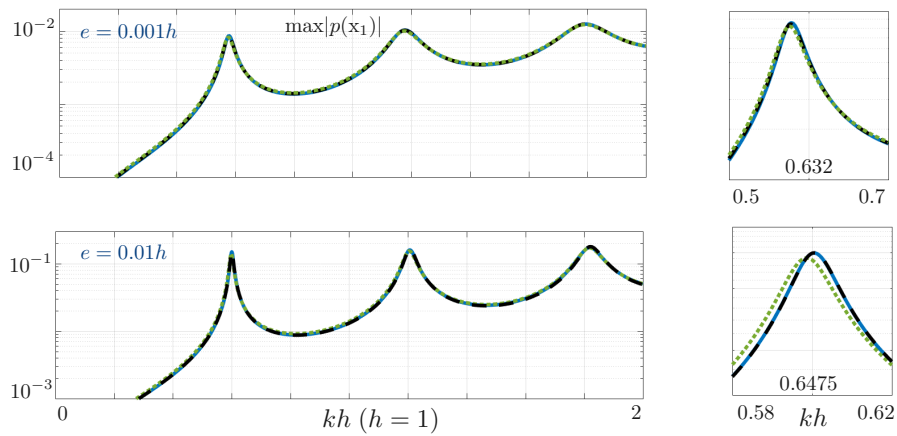


Figure 17: Validity of the thin wire approximation- same representation as in figure 5. Plain blue lines: direct numerics, dashed black lines: unified model with (29)-(30) and dotted green lines: Thin wire model with (29)-(58).